Investigation into Two Mechanisms of Unusual Decarboxylases: α-Amino-β-Carboxymuconate ε-Semialdehyde Decarboxylase and Orotidine 5'-Monophosphate Decarboxylase

by

Vanessa L. Smiley

Submitted in Partial Fulfillment of the Requirements

for the Degree of

Masters of Science

in the

Chemistry

Program

YOUNGSTOWN STATE UNIVERSITY

May, 2006

Investigation into Two Mechanisms of Unusual Decarboxylases:
α-Amino-β-Carboxymuconate ε-Semialdehyde Decarboxylase and
Orotidine 5'-Monophosphate Decarboxylase

Vanessa L. Smiley

I hereby release this thesis to the public. I understand that this thesis will be made available from the OhioLINK ETD Center and the Maag Library Circulation Desk for public access. I also authorize the University and other individuals to make copies of this thesis as needed for scholarly research.

Signature:

Vanessa L. Smiley, Student — Date: 5/4/06

Approvals:

Jeffrey A. Smiley, Thesis Supervisor — Date: 5/4/06

Daryl W. Mincey, Thesis Advisor — Date: 5/3/06

Thomas D. Kim, Committee Member — Date: 5/3/06

Michael A. Serra, Committee Member — Date: 5/3/06

Peter J. Kasvinsky, Dean of School of Graduate Studies & Research — Date: 5/5/06

ABSTRACT

ACMSD and ODCase are two different decarboxylase enzymes with mechanisms that deviate from the typical mechanisms found for these types of enzymes. Studying these enzymes may help elucidate these extraordinary mechanisms in which the substrate is converted to a product with carbon dioxide. Our group intends on producing recombinant mouse ACMSD for characterization and insight into ACMSD's mechanism. Because ACMS is unstable, the enzyme preceding ACMSD, 3-hydroxyanthranilate oxygenase (3-HAO) was used to produce the substrate. Alternate substrates for 3-HAO were tested in order to find a more stable substrate or inhibitor for ACMSD. ACMSD's mechanism is proposed to involve a Michael addition where a nucleophilic attack on the substrate is used to stabilize the carbanion formed.

The mechanism proposed for ODCase involves a zwitterionic intermediate using the active site lysine (Lys73 in *E. coli*) to protonate O2 on the pyrimidine ring of orotidine 5'-monophosphate (OMP) and then subsequent decarboxylation at C6. Using a semi-enzymatic synthesis of [^{18}O2, ^{13}C-*carboxyl*] OMP, analysis of ODCase can be performed by measuring carbon isotope effects for the decarboxylation reaction of natural abundance and specifically labeled substrate. Measurement of isotope effects involves collecting carbon dioxide produced by the reaction of OMP and ODCase and analysis of the CO_2 using an isotope ratio mass spectrometer. If the isotope effects produce significantly different values with the natural abundance and specifically labeled substrates, this would help support the mechanism proposed.

ACKNOWLEDGMENTS

I would like to thank Youngstown State University and all the people related to the university that helped me obtain both my degrees. I would like to especially thank Dr. Mike Serra, Dr. John Jackson and Dr. Ron Tabak for being great friends in addition to being associates of the university. Lastly, I thank my husband, Jeffrey Smiley, with whom I have performed the best research projects.

TABLE OF CONTENTS

LIST OF FIGURES

LIST OF TABLES

LIST OF SYMBOLS AND ABBREVIATIONS

α	alpha
β	beta
ε	epsilon
°C	degrees Celsius
g	gram
mL	milliliter
mM	millimolar
μM	micromolar
nm	nanometer
s	seconds
hr	hour
nmol	nanomoles
Abs	Absorbance
min	minute
μg	microgram
Amp	ampicillin

Chapter 1

Introduction to Decarboxylases

Typical Decarboxylases

Enzymology has progressed rapidly since the establishment of recombinant gene techniques. This has led to maximal protein production and significantly purer enzymes for various mechanistic studies. Many enzymes can now be characterized at a rapid rate including the mechanistically unusual enzymes in the decarboxylation category. Most decarboxylases require a component to stabilize an anionic intermediate. Some examples, as presented by Marion O'Leary [1], of common anionic stabilizers include metal-ion dependent, Schiff base catalyzed and β-ketoacid decarboxylation mechanisms.

Metal ion-dependent decarboxylases utilize metals (usually containing a charge greater than +1) to stabilize negatively charged groups on the substrate to assist in the stabilization of the transition state and the release of CO_2. As an example, oxaloacetate decarboxylase has been found to contain a manganese ion that is essential in converting oxaloacetate to CO_2 and pyruvate (Figure 1-1). The metal ion is used to stabilize the α-ketoacid present on one side while the carboxyl group, which is part of a β-ketoacid, is removed from the other end. Oxaloacetate can spontaneously decarboxylate *in vitro* at neutral pH with the addition of metal ions, but the reaction is also catalyzed with this metal ion-dependent decarboxylase.

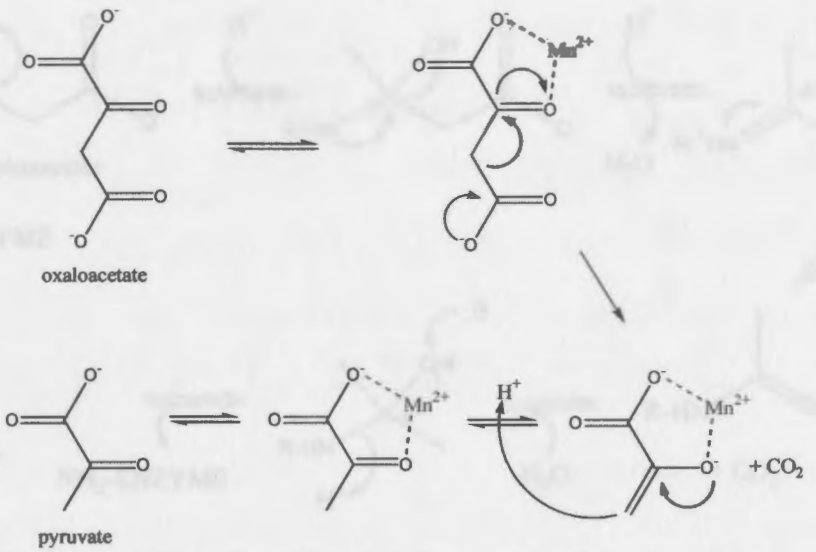

Figure 1-1. Metal-ion assistance of the decarboxylation of oxaloacetate to pyruvate and CO_2.

Schiff base catalyzed reactions use an amine group to create a more reactive intermediate and release the CO_2. The amine group can be found on the substrate, enzyme or an enzyme cofactor. Acetoacetate decarboxylase, for example, contains a lysine residue in the active site that assists the decarboxylation of acetoacetate to acetone (Figure 1-2). The terminal nitrogen on the lysine residue acts as an electron stabilizer to assist decarboxylation as well as the water catalysis involved in this particular mechanism.

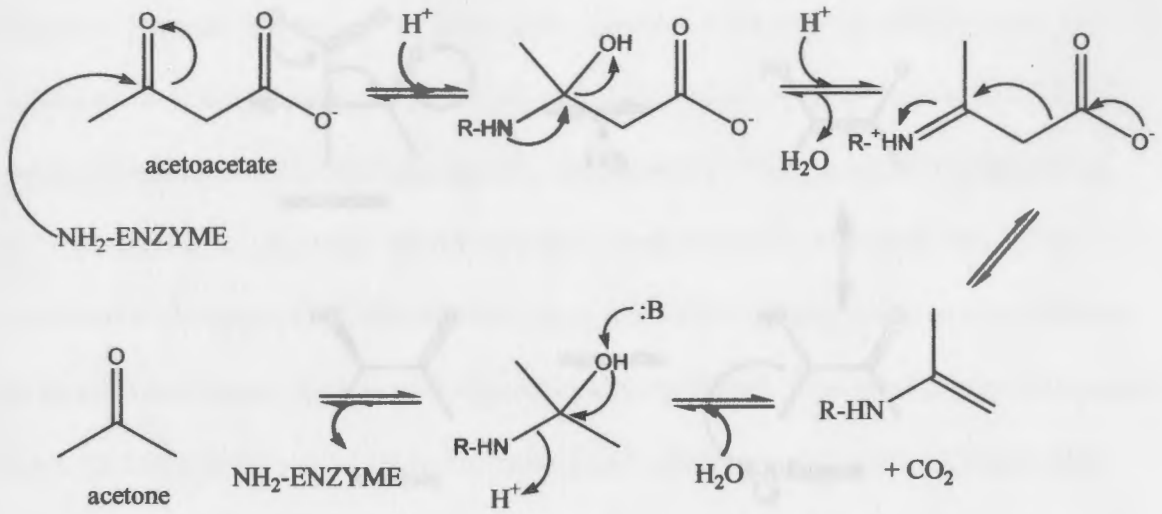

Figure 1-2. Decarboxylation of acetoacetate by acetoacetate decarboxylase. (R = the rest of the enzyme)

β-Ketoacids can easily decarboxylate with little assistance from an enzyme as seen previously where metal ions in solution can help decarboxylation. Acetolactate decarboxylase has no known metal ion or cofactor which the enzyme uses to stabilize its substrate but it can likely be attributed to internal stability of the substrate that the molecule can be decarboxylated with this particular enzyme (Figure 1-3). The enzyme likely assists as a proton donor and resonance stabilizer. It has been found to produce the stereochemical product *R*-acetoin, which means the proton donor is only contacting on one side of the molecule.

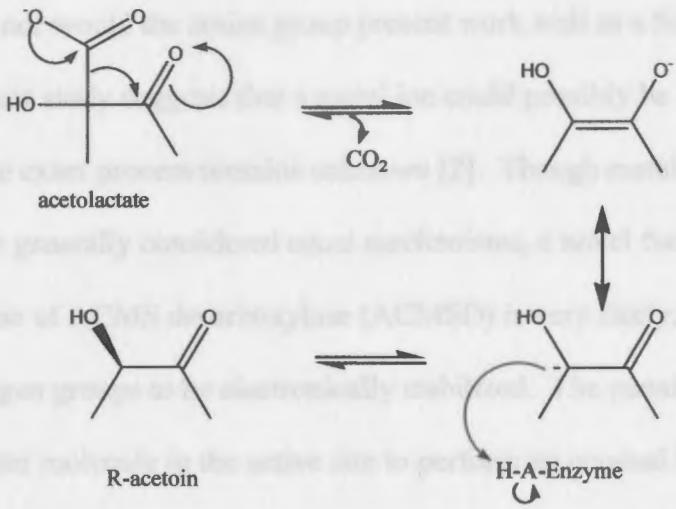

Figure 1-3. Mechanism of acetolactate decarboxylase.

Atypical Decarboxylase 1: α-Amino-β-Carboxymuconate ε-Semialdehyde Decarboxylase

The mechanisms that have been described are unlikely mechanisms for the two enzymes presented in this thesis. The first unusual decarboxylase utilizes α-amino-β-carboxymuconate ε-semialdehyde (ACMS) to produce α-aminomuconate ε-semialdehyde (AMS), which can non-enzymatically and spontaneously convert to picolinic acid (Figure 1-4). ACMS lacks a carbonyl group next to the labile carboxylate so it cannot react as a

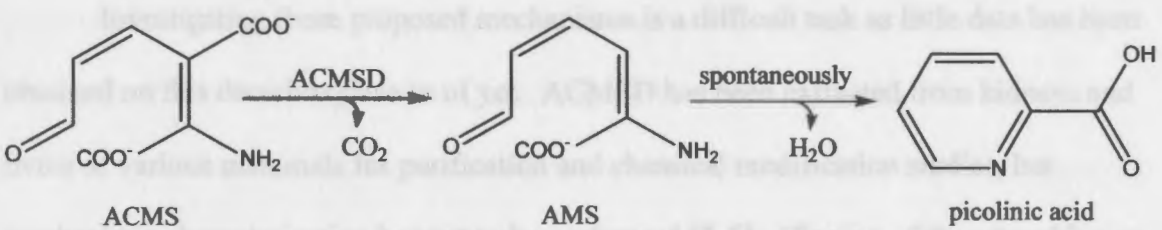

Figure 1-4. Conversion of ACMS to AMS via ACMSD.

β-ketoacid would, nor would the amine group present work well as a Schiff base. Evidence from a new study suggests that a metal ion could possibly be involved in the mechanism, but the exact process remains unknown [2]. Though metal ion dependent decarboxylases are generally considered usual mechanisms, a novel function for the metal ion in the case of ACMS decarboxylase (ACMSD) is very likely, as the substrate lacks adjacent oxygen groups to be electronically stabilized. The metal ion could be used to coordinate a water molecule in the active site to perform an unusual hydration that would activate the substrate and produce the decarboxylated product. Another possible mechanism for ACMSD includes a nucleophilic attack or Michael addition by the enzyme on the substrate to stabilize and produce decarboxylation (Figure 1-5).

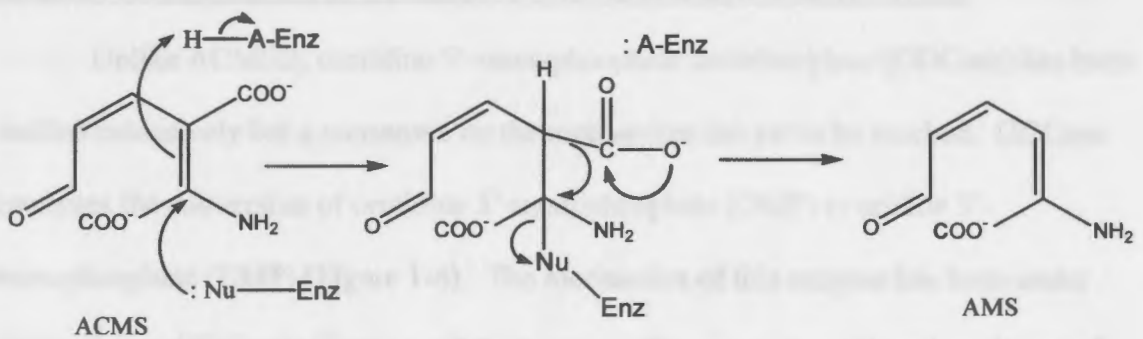

Figure 1-5. The proposed mechanism for ACMSD showing a nucleophilic attack leading to the decarboxylation of the substrate. The nucleophile in this mechanism could be a water molecule.

Investigating these proposed mechanisms is a difficult task as little data has been obtained on this decarboxylase as of yet. ACMSD has been extracted from kidneys and livers of various mammals for purification and chemical modification studies, but mechanistic characterization has yet to be performed [3-5]. Cloning of the rat and human ACMSD genes has been performed but the conclusions have been consistent with previous papers [6, 7]. All that can be inferred from these studies is that the addition of

$MgCl_2$ seems to increase activity, though metal chelating agents do not seem to inhibit the enzyme. Inhibition has been found using iodoacetamide as well as other chemical modifying agents that interfere with sulfur and nitrogen containing amino acids. The latest results by Li *et. al.* [2] showed that the substrate for ACMSD, when generated by 3-hydroxyanthranilate oxygenase (3-HAO), a non-heme ferrous ion dependent enzyme, may utilize the metal ion for catalysis. Though metal chelating agents do not seem to affect ACMSD activity, this does not mean that it could not use a divalent metal ion. This study found ACMSD to utilize iron, cobalt, cadmium and manganese metal ions to perform a nonoxidative decarboxylation. Therefore, neither mechanism (metal ion dependent or Michael addition) can be ruled out.

Atypical Decarboxylase 2: Orotidine 5'-monophosphate Decarboxylase

Unlike ACMSD, orotidine 5'-monophosphate decarboxylase (ODCase) has been studied extensively but a consensus on the mechanism has yet to be reached. ODCase catalyzes the conversion of orotidine 5'-monophosphate (OMP) to uridine 5'-monophosphate (UMP) (Figure 1-6). The mechanism of this enzyme has been under debate due to ODCase's highly proficient nature. The uncatalyzed decarboxylation of OMP is so slow, the resulting ratio of rates for the catalyzed vs. uncatalyzed reaction (k_{cat}/k_{uncat}) is extraordinarily high [8]. Therefore, various mechanisms have been proposed by a number of different groups with only a few of these mechanisms being ruled out. The various mechanisms, including the proposed mechanism for this thesis, will be briefly investigated based on a recent volume of *Topics in Current Chemistry* [9].

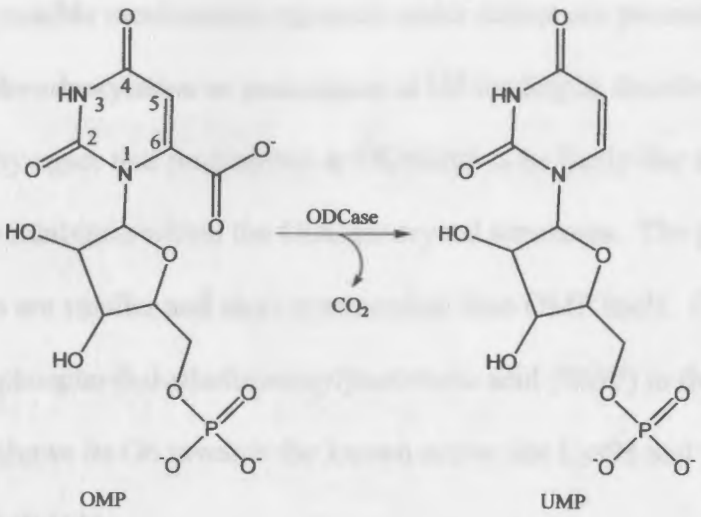

Figure 1-6. ODCase catalyzes the reaction of OMP to UMP.

Since 2000, several ODCase crystal structures have been published with and without inhibitors, but none with the actual substrate [10-13]. These crystal structures, along with isotope effect studies [14], have ruled out nucleophilic attack at the C5 of the pyrimidine ring as well as weaken the argument for protonation at C5 and O4 (Figure 1-7).

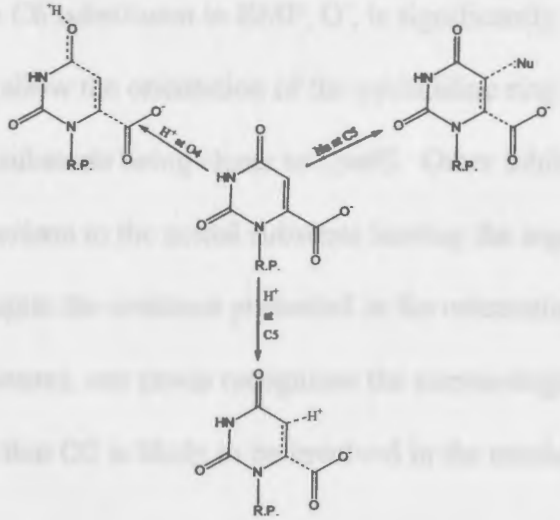

Figure 1-7. Protonation at O4 and C5 as well as nucleophilic attack at C5 are currently not considered possible mechanisms for ODCase though they were considered initially. (R.P. = ribose phosphate)

The two possible mechanisms currently under debate are protonation at C6 concurrent with decarboxylation or protonation at O2 leading to decarboxylation (Figure 1-8). The majority agree that protonation at C6 seems to be likely due to the binding orientation of the inhibitors within the ODCase crystal structures. The problem arises in that the inhibitors are smaller and more symmetrical than OMP itself. For example, binding of 1-(5'-phospho-β-d-ribofuranosyl)barbituric acid (BMP) in the yeast ODCase crystal structure shows its O6 towards the known active site Lys93 and O2 towards Gln215 (Figure 1-9) [11].

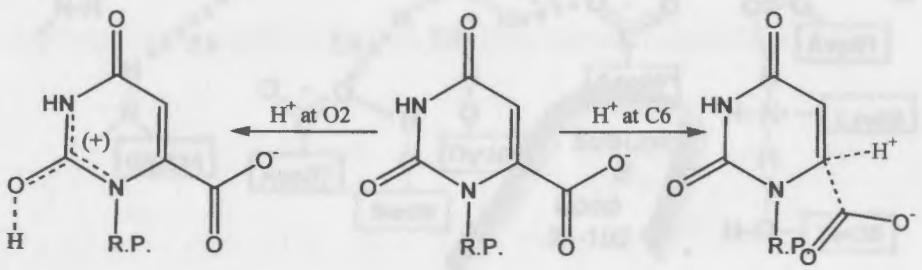

Figure 1-8. Protonation at O2 and C6 are two possible mechanisms currently in debate. (R.P. = ribose phosphate)

The size of the C6 substituent in BMP, O^-, is significantly smaller than the COO^- in OMP, which could allow the orientation of the pyrimidine ring to be flipped 180° resulting in O2 of the substrate being closer to Lys93. Other inhibitors present similar issues of size in comparison to the actual substrate leaving the argument of the actual mechanism open. Despite the evidence presented in the orientation of the inhibitors within the crystal structures, our group recognizes the enzymological data that shows the importance of O2 and that O2 is likely to be involved in the mechanism of ODCase.

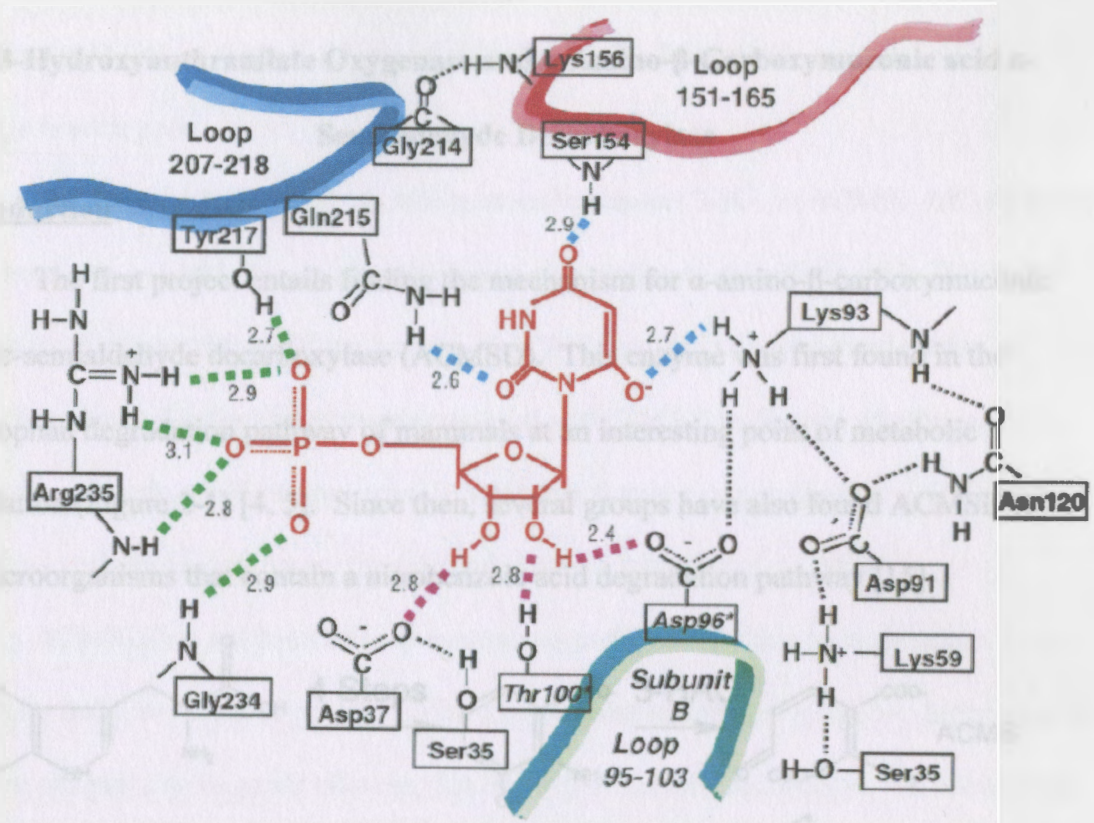

Figure 1-9. Binding of BMP in yeast ODCase active site from Miller *et al.*, *PNAS*, **2000**, 97, (5), 2011-6 [11].

Chapter 2

3-Hydroxyanthranilate Oxygenase and α-Amino-β-Carboxymuconic acid ε-Semialdehyde Decarboxylase

Introduction

The first project entails finding the mechanism for α-amino-β-carboxymuconic acid ε-semialdehyde decarboxylase (ACMSD). This enzyme was first found in the tryptophan degradation pathway of mammals at an interesting point of metabolic regulation (Figure 2-1) [4, 5]. Since then, several groups have also found ACMSD to be in microorganisms that contain a nitrobenzoic acid degradation pathway [15].

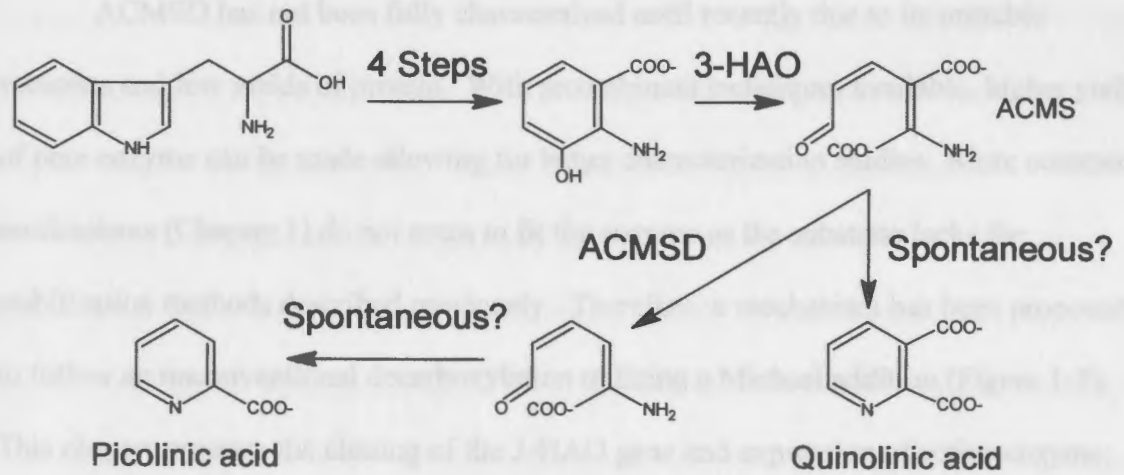

Figure 2-1. The tryptophan degradation pathway showing the conversion of ACMS to quinolinic or picolinic acid.

At the point where 3-hydroxyanthranilate oxygenase (3-HAO) converts 3-HA to ACMS, two possible steps can occur. Within minutes of its production ($t_{1/2} \approx 43$ minutes), ACMS can undergo a spontaneous, non-enzymatic reaction to quinolinic acid, which is then used in the NAD^+ biosynthetic pathway. If ACMS does not undergo the spontaneous reaction, the enzyme ACMSD can utilize it for decarboxylation into α-

aminomuconate ε-semialdehyde (AMS), which can also non-enzymatically cyclize into picolinic acid. A mechanistic study of ACMSD could elucidate the reason for this strange branch point.

To study ACMSD, 3-HAO will be used to convert 3-HA to ACMS. ACMS is not commercially available due to its non-enzymatic reaction to quinolinic acid. This step is necessary to generate a sufficient supply of ACMS for use in the enzymatic assay of ACMSD. Several other compounds were used with 3-HAO to discern whether an alternate substrate could be converted to a product that is more stable than ACMS and could potentially be used as an alternate substrate or inhibitor of ACMSD.

ACMSD has not been fully characterized until recently due to its unstable substrate and low yields of protein. With recombinant techniques available, higher yields of pure enzyme can be made allowing for better characterization studies. More common mechanisms (Chapter 1) do not seem to fit the enzyme as the substrate lacks the stabilization methods described previously. Therefore, a mechanism has been proposed to follow an unconventional decarboxylation utilizing a Michael addition (Figure 1-5). This chapter presents the cloning of the 3-HAO gene and expression of active enzyme; use of 3-HAO for synthesis of ACMS and investigation of the utilization of alternate substrates; production of ACMSD for the mechanistic study; and producing a useful ACMSD assay.

Materials and Methods

Cloning and Expression of 3-HAO in the Parent Plasmid pCAL-n

Previous to this thesis, the yeast 3-HAO gene was inserted into the pESP-1 expression vector, but was ineffective at producing large quantities of protein (Katie

Muzevich and Vanessa (Ho) Smiley, 2002-2003). The 3-HAO gene was amplified from this construct by PCR using primers designed for insertion into BamHI-SalI digested pCAL-n vector (Stratagene). The primers (Integrated DNA Technologies) have the following sequences with restriction sites underlined:

5' primer: 5'-GACGGCCAGTGGATCCATGTTTAATACTACACCAATTAAT-3'

3' primer: 5'-CGACTCTAGAGTCGACTTAATTAGATTGAGGGCGTGCGTA-3'

Amplification reactions were carried out with Vent® DNA polymerase (New England Biolabs; also the source for DNA modifying enzymes below) according to the manufacturer's recommendations. Thermal cycles were as follows: 35 cycles of the following three steps: 95 °C for 90 s, 55 °C for 30 s, 75 °C for 90 s; and a final 75 °C for a 4 min period. The PCR product was purified, digested with BamHI and SalI restriction endonucleases, and ligated to BamHI and SalI-digested pCAL-n (Stratagene) with T4 DNA ligase. The recombinant plasmid was then transformed into BL21 (DE3) Gold (Stratagene) cells (hereafter referred to as "BL21 cells"). Transformation was performed by calcium chloride treatment of BL21 cells, addition of pCAL-3HAO ligated plasmid, recovery in LB medium at 37 °C with shaking and subsequent plating on LB/Amp plates for growth at 37 °C overnight. Potential plasmids with the desired insert were identified in mini-plasmid preparations from individual colonies arising after the transformation. Several potential positives were further purified and the presence of the insert was verified by restriction digest (as above) and agarose gel electrophoresis. The sequence of the insert was verified by DNA sequencing (Beckman and Coulter CEQ DTCS kit and CEQ 2000XL DNA Analysis System) to ensure restriction sites were intact and that the desired insert was present.

Expression of the calmodulin-binding peptide (CBP) tagged 3-HAO protein was performed by growth of the BL21 cells containing the pCAL-3HAO plasmid in LB/Amp, overnight at 37 °C with shaking. A secondary culture of LB/Amp plus 0.1 mM ferrous sulfate was inoculated with a 1:100 dilution of the overnight culture and incubated at 37°C with shaking for 3 h. Induction for protein production occurred with the addition of isopropyl-β-D-thiogalactopyranoside (IPTG) to a final concentration of 0.8 mM and subsequent growth at 37 °C with shaking for 4 h.

The cells were harvested by centrifugation and then resuspended in 800 µL per 50 mL of original cell culture of a buffered solution containing 10 mM HEPES, pH 6.5, 1.0 mM dithiothreitol (DTT), 0.3 mM ferrous sulfate, 1.0 mM phenylmethylsulfonyl fluoride (PMSF), 1 µM pepstatin A and 100 µM leupeptin. The cells were lysed using the Mini Bead Beater (BioSpec Products) with 0.1 mm glass beads using three 1-min pulses at high speed, interspersed with periods of cooling (at least 60 s) the lysate on ice. Centrifugation at 13,000 rpm for 5 min in an Eppendorf microcentrifuge was used to remove cell debris and the assay for crude 3-HAO activity was made. Purification was performed according to manufacturer's protocol (Stratagene). Protein size and solubility was observed by SDS-PAGE.

Activity Assays of 3-HAO for ACMS Production and use of Potential Alternate Substrates

Protein concentration was determined using Bradford reagent (Bio-Rad) and bovine serum albumin (Pierce) as a standard. Assays were performed spectrophotometrically (HP diode array 8453) observing the increase of absorbance at 360 nm [5]. A solution of 3-HA with a concentration of approximately 1 mM, in 10 mM HEPES, pH 6.5, was prepared immediately before the assay. Exact concentration of

3-HA was determined spectrophotometrically at 315 nm with $\varepsilon = 3240\ M^{-1}$. The 1.0 mL assay mixture contained a final concentration of 10 mM HEPES, pH 6.5, 0.1 mM ferrous sulfate, 1.0 mM DTT, cell lysate and 3-HA or alternate substrate. The assay was initiated by the addition of 3-HA (or alternate substrate) and absorbance was recorded every 10 s for a total of 70 to 280 s. Specific activity was determined using the 100 μM 3-HA assay. A K_m value was determined using concentrations from 16.7 μM to 100 μM 3-HA. Solutions of the potential alternate substrates were prepared in the same concentration and buffer as 3-HA.

Cloning and Expression of ACMSD in the Parent Plasmid pCAL-n

The mouse ACMSD (Resgen, IMAGE clone ID 4235456) was amplified by PCR using primers designed for insertion into NdeI-SalI digested pCAL-n vector. The primers (Integrated DNA Technologies) have the following sequences with restriction sites underlined:

5' primer: 5'- ACAGTAGACTCATATGAAAATTGACATCCACACTCAT -3'

3' primer: 5'- ACATGGTACGGTCGACTCATTCAAATAGTTTTCCAAG -3'

Amplification reactions were carried out with Vent® DNA polymerase according to the manufacturer's recommendations. Thermal cycles were as follows: 35 cycles of the following three steps: 95 °C for 90 s, 55 °C for 30 s, 75 °C for 90 s; and a final 75 °C for a 4 min period. The PCR product was purified, digested with NdeI and SalI restriction endonucleases, and ligated to NdeI and SalI-digested pCAL-n with T4 DNA ligase. The recombinant plasmid was then transformed into BL21 cells. Transformation was performed by calcium chloride treatment of BL21 cells, addition of pCAL-ACMSD ligated plasmid, recovery in LB medium with 2% glucose at 37 °C with shaking and

subsequent plating on LB/Amp with 2% glucose plates for growth at 37 °C overnight. Potential plasmids with the desired insert were identified in mini-plasmid preparations from individual colonies arising after the transformation. Several potential positives were further purified and the presence of the insert was verified by restriction digest (as above) and agarose gel electrophoresis. The sequence of the insert was partially verified by DNA sequencing to ensure restriction sites were intact and that the desired insert was present.

Optimal conditions for expression of the ACMSD protein was performed by growth overnight at 37°C with shaking of the BL21 cells containing the pCAL-ACMSD plasmid in LB/Amp. A secondary culture of 2xYT (yeast extract and tryptone) plus 0.1 % glucose was inoculated with a 1:100 dilution of the overnight culture and incubated at 37 °C with shaking for 3 h. Induction for protein production occurred with the addition of IPTG to a final concentration of 0.1 mM and subsequent growth at 20 °C or room temperature with shaking for 2 h. The cells were harvested by centrifugation and then resuspended in 800 µL per 50 mL of original cell culture of a buffered solution containing 10 mM HEPES, pH 6.5, 1.0 mM DTT, 1.0 mM PMSF, 1 µM pepstatin A and 100 µM leupeptin. The cells were lysed using the Mini Bead Beater with 0.1 mm glass beads using three 1-min pulses at high speed, interspersed with periods of cooling (at least 60 s) the lysate on ice. Centrifugation at 13,000 rpm for 5 min in a microcentrifuge was used to remove cell debris and the assay for crude ACMSD activity was made. Protein size and solubility was observed by SDS-PAGE.

Activity Assays of ACMSD

Protein concentration was determined using Bradford reagent and bovine serum albumin as a standard. Assays were performed as described previously for 3-HAO with the following modifications: 3-HA final concentration was limited to 20 μM; when sufficient 3-HAO was added, the solution reached a final absorbance of ~0.74 at 360 nm. The solution with this new absorbance was presumed to be 20 μM ACMS. Crude ACMSD protein was added after the absorbance reached 0.74 and activity was detected by a decrease in the absorbance. An assay without ACMSD was performed to determine the amount of spontaneous absorbance decrease, attributable to the conversion of ACMS to quinolinic acid. Specific activity was determined at 20 μM 3-HA.

Results and Conclusions

The plasmid resulting from ligation of pCAL-n with the 3-HAO PCR product was approximately 6.3 kbp compared to the original pCAL-n vector of 5.8 kbp. Restriction digestion of the Qiagen purified, potential pCAL-3-HAO plasmid showed two bands around 5.8 kbp and 0.5 kbp (data not shown). DNA sequencing of the 5' end of the potential plasmid shows both restriction sites intact as well as the entire 3-HAO gene (Appendix A).

Expression of 3-HAO was originally performed in LB media, but the addition of Fe^{+2} ions helped stabilize the enzyme for storage purposes. The expression system used was highly successful in producing large quantities of protein with a size of ~24 kDa (Figure 2-2). The expected size of 3-HAO is 20.2 kDa but the CBP fusion tag adds 4 kDa.

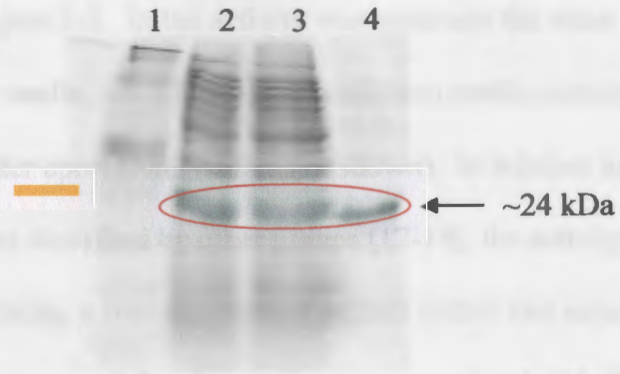

Figure 2-2. SDS-PAGE of 3-HAO.
Lane 1: Kaleidoscope molecular weight markers (Bio-Rad).
Lane 2: 3.6 μg crude 3-HAO.
Lane 3: 15 μL of protein flow through.
Lane 4: Purified, concentrated 3-HAO. 3-HAO protein (circled in red) can be seen just below the 30.6 kDa marker. The orange band represents where the 30.6 kDa marker should be seen.

The success of purification of the CBP tagged 3-HAO was limited, which can also be seen in Figure 2-2. Using the CBP fusion tag, only a small quantity of purified protein could be retained due to the amount and expense of the CBP resin. Once purified, 3-HAO was also made inactive by the use of EGTA in the elution buffer. Even dialysis and addition of Fe^{+2} ions to attempt to reactivate the protein (described previously by Koontz and Shiman [16]) did not seem to improve the activity of the purified enzyme. However, purification should not be necessary for our purpose of generating ACMS, because *E. coli* have not been found to contain 3-HAO activity, and there should not be any enzyme activity present that would convert ACMS to any other product. Therefore, only crude 3-HAO was utilized in the assays performed for both 3-HAO and ACMSD.

The crude 3-HAO was found to have a specific activity of 0.464 $nmol \cdot min^{-1} \cdot \mu g^{-1}$ and a K_m of 54 μM using HEPES buffer at pH 6.5. The highest specific activity obtained with the yeast 3-HAO was found using sodium phosphate buffer at pH 6.5 (0.475 $nmol \cdot min^{-1} \cdot \mu g^{-1}$). A sample of spectrophotometric data obtained during a 3-HAO assay

can be seen in Figure 2-3. Initial activity was relatively the same with or without Fe^{+2} ions added to the media, but 3-HAO produced from media containing Fe^{+2} seemed to retain activity better upon storage (data not shown). In relation to the activity of varying recombinant genes described by other groups [17-19], the activity of our yeast 3-HAO is sufficient in producing a concentration of ACMS within two minutes, which is necessary to minimize the amount of absorbance decrease associated with the spontaneous reaction to quinolinic acid (Table 2-1).

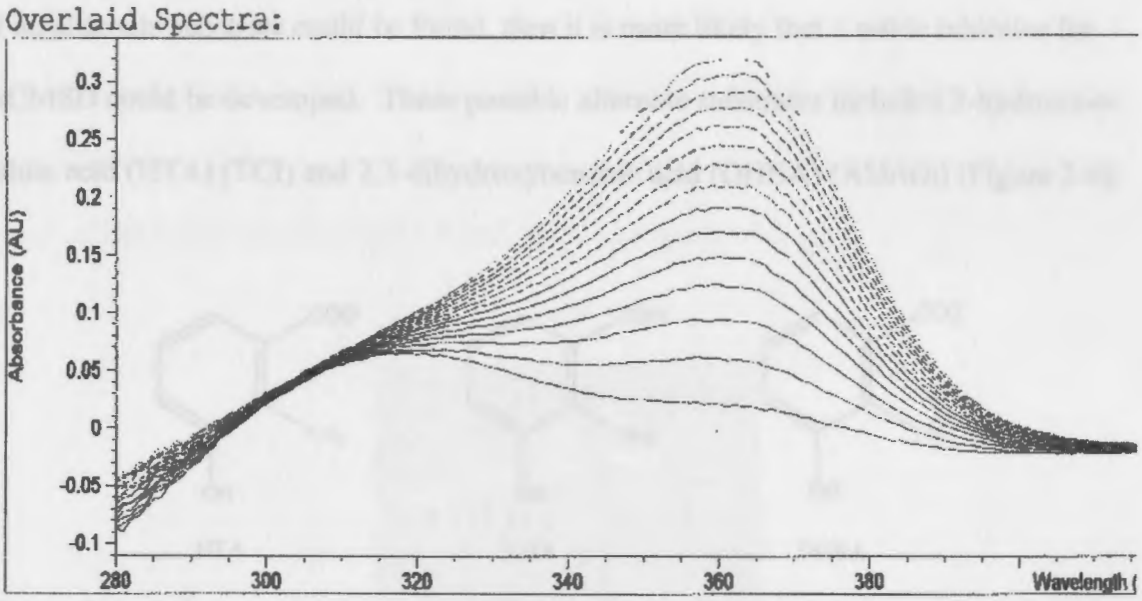

Figure 2-3. Spectrophotometric assay of the conversion of 3-HA to ACMS at 360 nm. Spectrum with lowest absorbance occurs at time zero; spectra with progressively higher absorbances were taken every ten seconds.

Reference	Source of 3-HAO gene	Expression System	Specific Activity (nmol·min^{-1}·μg^{-1})
Our Study	Yeast	BL-21 (DE3) Gold *E.coli*	0.464 (crude lysate)
[17]	Human	HEK-293 tissue	0.14/0.19 (crude lysate)
[18]	Human	BL-21 (DE3) *E.coli*	120**
[19]	*R. metallidurans*	Tuner (DE3) *E.coli*	16 (gel-filtration purified)

Table 2-1. Comparison of different 3-HAO studies in relation to genetic source, expression system and specific activity. **Main source of crude protein was reported as inclusion bodies.

Assays were also performed using two potential alternate substrates for 3-HAO. If an alternate substrate could be found, then it is more likely that a stable inhibitor for ACMSD could be developed. These possible alternate substrates included 3-hydroxy-*o*-toluic acid (HTA) (TCI) and 2,3-dihydroxybenzoic acid (DHBA) (Aldrich) (Figure 2-4).

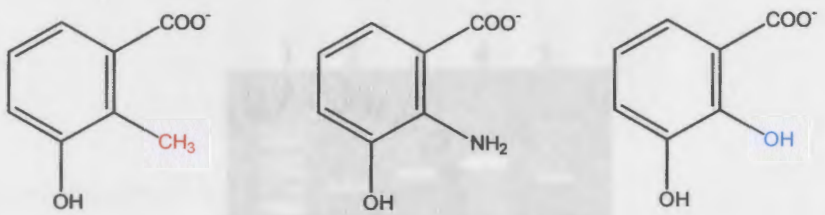

HTA 3-HA DHBA

Figure 2-4. 3-Hydroxy-*o*-toluic acid (HTA) has a methyl group substituted and 2,3-dihydroxybenzoic acid (DHBA) has a hydroxyl group substituted for the amino group on 3-HA.

Both compounds were tested under conditions similar to 3-HA where 3-HAO was produced in phosphate buffered saline (PBS), pH 7.4, instead of HEPES, pH 6.5 with all other additives the same. Assay conditions contained a final concentration of 10 mM Tris-acetate, pH 8.0 or 10 mM sodium phosphate, pH 6.5 instead of HEPES, pH 6.5 with all other components the same. Though the cell lysis and reaction conditions varied from the optimal found (HEPES buffer being better than one containing phosphate that could

potentially inhibit protein activity of ACMSD), protein activity was measurable when using 3-HA. However, assays with the two other compounds showed no measurable absorbance change upon addition of 3-HAO, indicating a lack of measurable reaction toward these two potential alternate substrates. Neither HTA nor DHBA served as a suitable alternate substrate for 3-HAO.

Cloning of the mouse ACMSD gene was performed initially with the CBP fusion tag using BamHI and SalI restriction sites. Once the efficiency of the purification system was found to yield only small quantities of purified protein, the gene was recloned using NdeI and SalI, which excluded the CBP fusion tag in the protein expression. A plasmid approximately 6.8 kbp was found and could be digested with endonucleases to yield two bands of DNA with sizes around 5.8 and 1.0 kbp (Figure 2-5).

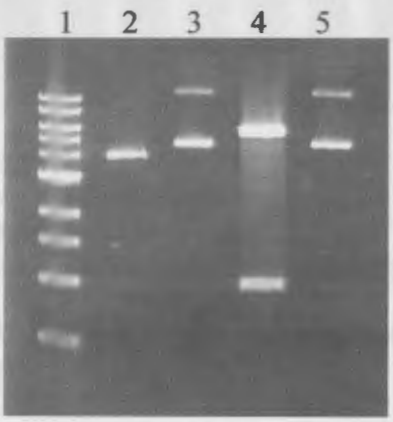

Figure 2-5. Restriction digested pCAL-ACMSD using NdeI and SalI endonucleases on 0.8% agarose gel.
Lane 1: DNA molecular weight markers (Amresco).
Lane 2: 200ng uncut pCAL-n vector.
Lane 3: 200ng uncut pCAL-ACMSD plasmid.
Lane 4: 1 μg digested pCAL-ACMSD plasmid.

Though DNA sequencing was not performed to confirm the entire gene, a portion of the sequence including restriction sites were found to be present (Appendix B). This data was sufficient to proceed to expression of the protein.

Expression of ACMSD in the whole cells proved to be better than expression of 3-HAO comparative to induction time and IPTG concentration, but unfortunately the protein solubility was limited. The mouse ACMSD has an expected weight of 38 kDa and was easily seen after two hours of induction in the whole cell pellets (Figure 2-6).

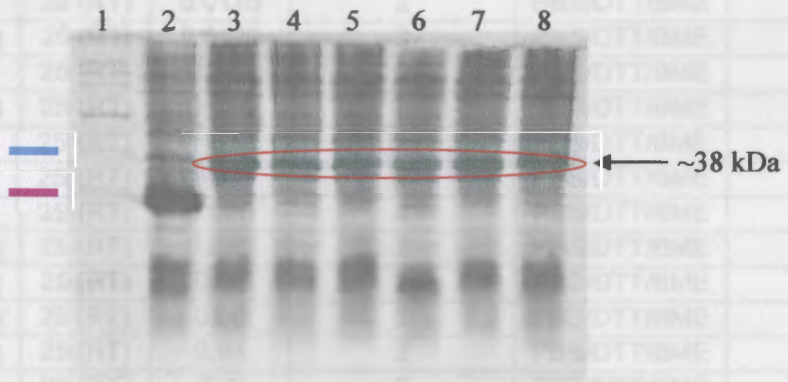

Figure 2-6. Expression of recombinant ACMSD.
Lane 1: Prosieve® color protein markers (Cambrex).
Lane 2: 10 μL of whole cell pellets for 3-HAO
Lanes 3-8: 10 μL of whole cell pellets for ACMSD expressed in condition 7(a-f) (Table 2-2), respectively.
The blue line represents the 42 kDa marker and the pink line represents the 27 kDa marker. ACMSD is circled in red for all six conditions.

Many trials involving changes in expression and lysis conditions were made with only limited success in producing soluble protein (Table 2-2 and Appendix C). Though a small amount of protein appeared to be soluble in conditions 4 through 7 by SDS-PAGE and active protein was assayed in conditions 6 and 7, the quantity of insoluble ACMSD was significantly greater (>90%) (Figures 2-6 and 2-7).

Condition	Media	Temp. (oC)	IPTG (mM)	Time Induced (hrs)	Lysis Buffer	Soluble ACMSD?
Initial	LB	37	0.2	0, 2, 4, and 6	PBS	No
1a	LB	25 (RT)	0.2	0, 2, 4, and 6	PBS	No
1b	LB/G	25 (RT)	0.2	0, 2, 4, and 6	PBS	No
2	LB	16-18	0.2	0, 2, 4, and 6	PBS	No
3a	LB	37	0.2	2	PBS/DTT/BME	No
3b	LB	25 (RT)	0.2	2	PBS/DTT/BME	No
3c	LB	37	0.1	2	PBS/DTT/BME	No
3d	LB	25 (RT)	0.1	2	PBS/DTT/BME	No
3e	LB	37	0.05	2	PBS/DTT/BME	No
3f	LB	25 (RT)	0.05	2	PBS/DTT/BME	No
3g	LB	37	0.025	2	PBS/DTT/BME	No
3h	LB	25 (RT)	0.025	2	PBS/DTT/BME	?
4a	LB	25 (RT)	0.025	2	PBS/DTT/BME	?
4b	2xYT/g	25 (RT)	0.025	2	PBS/DTT/BME	?
4c	LB	25 (RT)	0.0125	2	PBS/DTT/BME	?
4d	2xYT/g	25 (RT)	0.0125	2	PBS/DTT/BME	?
4e	LB	25 (RT)	0.005	2	PBS/DTT/BME	?
4f	2xYT/g	25 (RT)	0.005	2	PBS/DTT/BME	?
4g	LB	25 (RT)	0	2	PBS/DTT/BME	No
4h	2xYT/g	25 (RT)	0	2	PBS/DTT/BME	No
5a	LB	25 (RT)	0.025	2	PBS/DTT/BME	?
5b	2xYT/g	25 (RT)	0.025	2	PBS/DTT/BME	?
5c	2xYT/g	25 (RT)	0.04	2	PBS/DTT/BME	?
5d	2xYT/g	25 (RT)	0.06	2	PBS/DTT/BME	?
5e	2xYT/g	25 (RT)	0.08	2	PBS/DTT/BME	?
5f	2xYT/g	25 (RT)	0.1	2	PBS/DTT/BME	?
6a	LB	20 (RT)	0.025	2	HEPES/DTT/PI	Yes
6b	2xYT/g	20 (RT)	0.025	2	HEPES/DTT/PI	Yes
6c	2xYT/g	20 (RT)	0.04	2	HEPES/DTT/PI	Yes
6d	2xYT/g	20 (RT)	0.06	2	HEPES/DTT/PI	Yes
6e	2xYT/g	20 (RT)	0.08	2	HEPES/DTT/PI	Yes
6f	2xYT/g	20 (RT)	0.1	2	HEPES/DTT/PI	Yes
7a	LB	18 (RT)	0.025	2	HEPES/DTT/PI	Yes
7b	LB	18 (RT)	0.2	2	HEPES/DTT/PI	Yes
7c	2xYT/g	18 (RT)	0.08	2	HEPES/DTT/PI	Yes
7d	2xYT/g	18 (RT)	0.1	2	HEPES/DTT/PI	Yes
7e	2xYT/g	18 (RT)	0.15	2	HEPES/DTT/PI	Yes
7f	2xYT/g	18 (RT)	0.2	2	HEPES/DTT/PI	Yes

Table 2-2. Variation of expression conditions for ACMSD. IPTG was added to a final concentration of the listed value. RT = room temperature, g = 0.1 % glucose, G = 10 % glycerol, BME = 2-mercaptoethanol, and PI = protease inhibitor cocktail used in our lab. Soluble ACMSD protein denotes visible protein bands in lysate seen on SDS-PAGE.

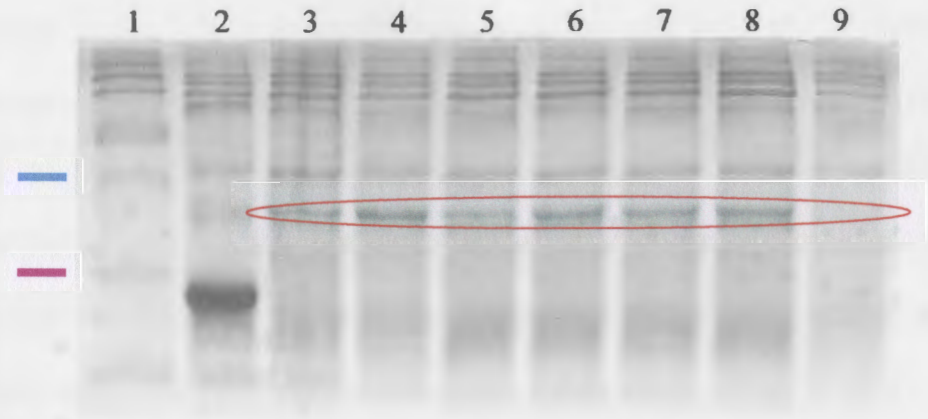

Figure 2-7. SDS-PAGE gel showing solubility of crude cell lysates for 3-HAO and ACMSD.
Lane 1: Prosieve® color protein markers.
Lane 2: 10 μg of crude lysed protein for 3-HAO
Lanes 3-8: 10 μg of crude lysed protein for ACMSD produced under condition 7(a-f)
Lane 9: Crude lysate protein for uninduced ACMSD, respectively.
ACMSD is circled in red. The blue and pink lines represent the 42 and 27 kDa markers, respectively.

The specific activity obtained was 1.36 $nmol \cdot min^{-1} \cdot \mu g^{-1}$ using HEPES buffer at pH 6.5 (Figure 2-8). Extraction of ACMSD for purification and reconstitution by addition of 8 M urea was accomplished; however, the protein recovered after dialysis was inactive (data not shown). Other studies of ACMSD have shown that extraction from liver and kidney sources produces small amounts of activity that must be purified in order to increase their specific activity, but recombinant *P. fluorescens* ACMSD has comparable activity to our recombinant mouse ACMSD just as crude protein lysate (Table 2-3) [2, 3, 5, 7, 15]. The activity of the *P. fluorescens* ACMSD with the addition of Fe^{+2} is important to see as the metal ion appears to increase the activity of ACMSD. This may be true of our mouse ACMSD as our assays include Fe^{+2} ions for 3-HAO. The presence of Fe^{+2} ions may also be increasing the activity of our enzyme.

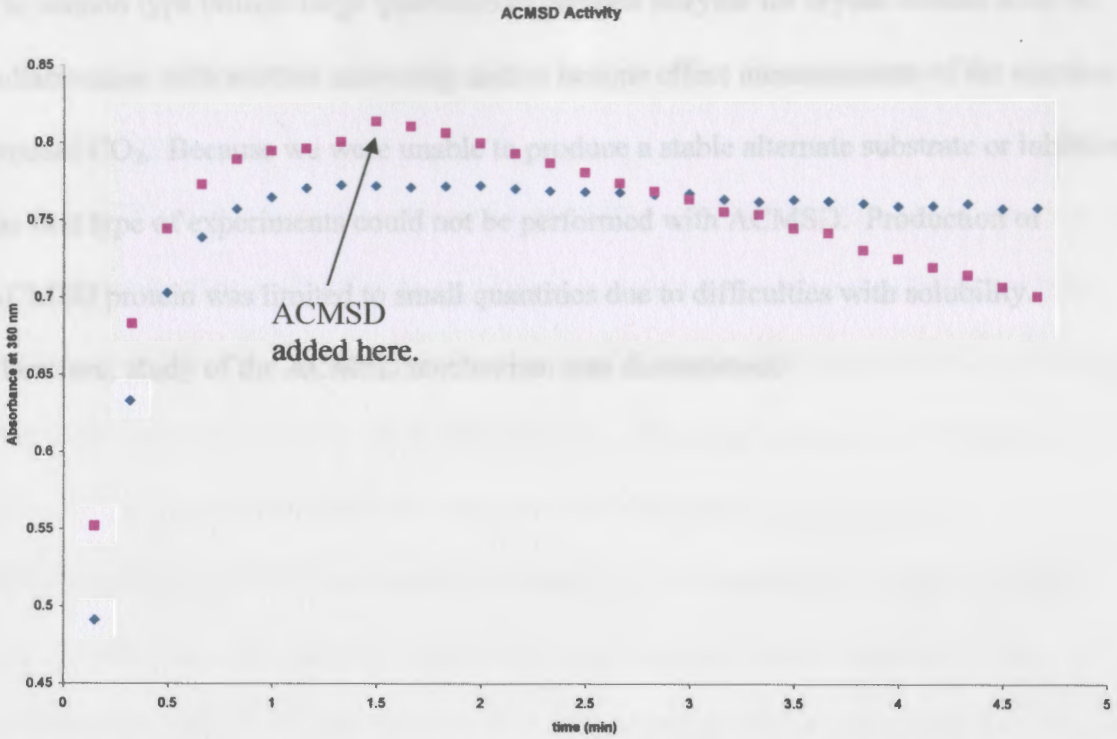

Figure 2-8. Activity assay for ACMSD from condition 7d. The blue dots represent the assay without enzyme, whereas the pink dots show the assay with crude ACMSD added.

Reference	Source of ACMSD gene	Expression System	Specific Activity ($nmol \cdot min^{-1} \cdot \mu g^{-1}$)
Our Study	Mouse	BL-21 (DE3) Gold *E.coli*	1.36 (crude lysate)
[5]	Cat	Liver Extract	0.0038 (homogenate)
[3]	Hog	Kidney Extract	0.0017 (homogenate)
[7]	Rat	Liver Extract	0.0018 (homogenate)
[7]	Rat	Kidney Extract	0.0046 (homogenate)
[15]	*P. fluorescens*	BL-21 *E.coli*	0.195 (crude lysate)
[2]	*P. fluorescens*	BL-21 (DE3) *E.coli*	2.9 (Fe^{+2} added**)

Table 2-3. Comparison of different ACMSD studies in relation to genetic source, expression system and specific activity. **ACMSD was purified with EGTA added to the buffer and then the metal ion was added into the assay mixture to ensure only one type of metal ion was used by the enzyme.

Our lab conducts two types of experiments. The first type involves experiments where small quantities of protein are used with alternate substrates or inhibitors (which can be isotopically enriched) to perform spectrophotometric assays and NMR analysis.

The second type utilizes large quantities of purified enzyme for crystal studies done in collaboration with another university and/or isotope effect measurements of the reaction product CO_2. Because we were unable to produce a stable alternate substrate or inhibitor, the first type of experiments could not be performed with ACMSD. Production of ACMSD protein was limited to small quantities due to difficulties with solubility. Therefore, study of the ACMSD mechanism was discontinued.

Chapter 3

Synthesis of Isotopically Enriched OMP for Enzymatic Studies

Introduction

ODCase catalyzes the conversion of OMP to UMP, which is an important step in the *de novo* synthesis of pyrimidines. This conversion is significant to DNA and RNA nucleotide synthesis. The mechanism used by ODCase has been under much speculation due to the enzyme's remarkable proficiency [8]. The $(k_{cat}/K_m)/k_{uncat}$ has been found to be 2.0×10^{23} M^{-1}, which is significant since the non-enzymatic, spontaneous decarboxylation of OMP is virtually undetectable. As discussed in Chapter 1, many mechanisms have been proposed, but a few mechanisms remain in question. The proposed mechanism for this thesis involves protonation at O2 on the pyrimidine ring and then subsequent decarboxylation at position 6. This zwitterionic formation is speculated to be assisted by the active site lysine (Lys93 in yeast and Lys73 in *E. coli*) as the proton donor.

This mechanism is proposed based on the published crystal structures [10-13]. Because ODCase reacts so quickly with OMP, the substrate has not been available for crystallography. Therefore, only inhibitors have been used with the enzyme to help elucidate the mechanism. A potential problem with this use is that the binding of the inhibitors may not be the same for the actual substrate. The space available for the pyrimidine ring is large enough to accommodate 180° ring flipping by rotation about the glycosidic bond for the inhibitors UMP and BMP because their position 6 groups (H and O^-, respectively) are smaller than the carboxyl group contained in the substrate. What can be seen in the positioning of the inhibitors within the active site is that the amount of

space provided by the active site glutamine (left of the pyrimidine, Figure 1-9) is larger than the space opposite provided by the active site lysine (right of the pyrimidine, Figure 1-9). Enough room in the active site is present so that the carboxyl group connected to C6 could be coordinated to the glutamine rather than the lysine due to size constraints.

Because we are unable to produce crystal structures containing the substrate, a method of isotopically enriching OMP can be used to help elucidate the mechanism of ODCase. Smiley *et al.* [14] described the first set of ^{13}C kinetic isotope effect data showing the effect of pH and glycerol content on the normal substrate using the yeast ODCase. As the pH was lowered, the kinetic isotope effect becomes greater. Another experiment utilizing OMP in deuterated water versus regular water as a solvent showed an increase in the ^{13}C kinetic isotope effect suggesting that the mechanism of protonation and subsequent decarboxylation is stepwise, not concerted [20].

The project for this thesis is to examine the oxygen isotope effect at O2 on the carbon isotope effect of decarboxylation. This experiment requires a method described by O'Leary [21] where the substrate can be doubly enriched. Heavy isotope enrichment can be made at a key position – in our case, O2 – where a reaction is thought to occur as well as enrichment at a position that can be easily detected by instrumentation – in our case, the carboxylate carbon. Stable isotopes have been found to produce more accurate results than radioactive isotopes so data analysis can be performed using an isotope ratio mass spectrometer (IR-MS). Therefore, enrichment of OMP can be done with ^{18}O at O2 (key position) and ^{13}C in the carboxylate (indicator position) (Figure 3-1). When this doubly enriched material is synthesized, it is mixed at a ratio of 1:90 with isotopically

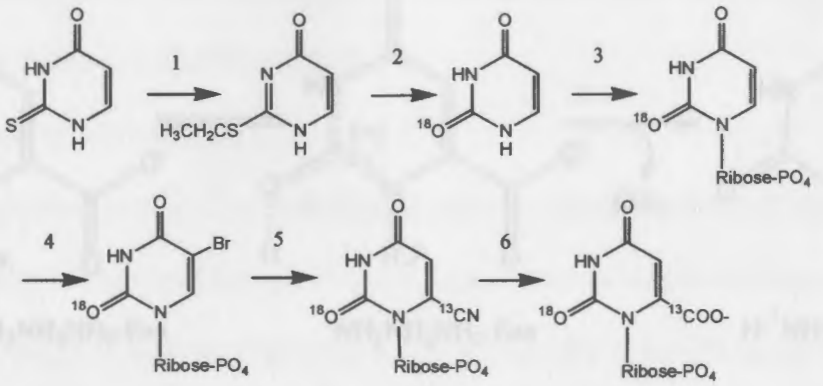

Figure 3-1. Synthetic scheme to produce [^{18}O2, ^{13}C-*carboxyl*]-OMP.

depleted OMP (synthesized using natural abundance oxygen in O2 and ^{13}C-depleted carbon for the carboxylate). Once the enzymatic decarboxylation occurs, the CO_2 can be collected and analyzed using the IR-MS; data from the IR-MS is then used to calculate the carbon kinetic isotope effect. The value for the carbon kinetic isotope effect for doubly enriched OMP will be equal to the equilibrium isotope effect of the protonation times the kinetic isotope effect for decarboxylation. If protonation does not occur at O2, the equilibrium isotope effect will equal 1.000 and the two kinetic isotope effects will be equal to each other. If protonation occurs at position O2 (Figure 3-2), the kinetic isotope effect for the doubly enriched OMP will be less than the value compared to the unenriched substrate. A typical equilibrium isotope effect for oxygen protonation is 0.985 [22]. Therefore, a kinetic isotope effect of 1.035 with natural abundance OMP would correspond to a value of 1.019 with the doubly enriched OMP. This difference should be easily measurable since values obtained using IR-MS should give errors of less than 0.002. This chapter includes the details for synthesis of [^{18}O2, ^{13}C-*carboxyl*]-OMP as well as information on ODCase assays used for CO_2 distillation and analysis by IR-MS.

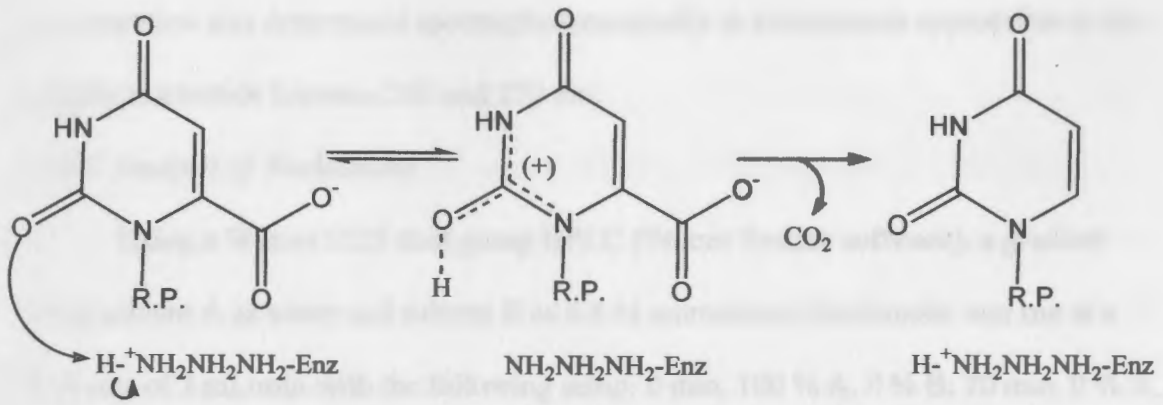

Figure 3-2. The proposed reaction catalyzed by ODCase, which may occur stepwise, where protonation of O2 occurs as an equilibrium and the formation of product is an irreversible step. If protonation occurs at O2, a significant difference in the kinetic isotope effects would be expected in the natural abundance OMP versus the [^{18}O2, ^{13}C-*carboxyl*]-OMP mixture.

Materials and Methods

Purification of Nucleotides by Anion Exchange Chromatography

Each nucleotide synthesized was applied to a column (2.5 cm diameter and lengths from 20 to 28 cm) filled with Dowex 1x8-200 anion exchange resin (Sigma/Aldrich) washed with 0.8 M ammonium bicarbonate and rinsed with dH_2O. A gradient from 0 to 0.8 M ammonium bicarbonate was used to separate out impurities. Reactions performed in organic solvents were washed with dH_2O before the gradient was applied to remove solvent. Fractions were analyzed by UV absorbance between 260 and 270 nm and subsequently by HPLC (as described below). Fractions containing the desired nucleotide were pooled and desalted with Dowex HCR-W2 cation exchange resin (Sigma/Aldrich), which was washed prior to desalting with 1 M HCl and then rinsed with dH_2O, until the eluate was neutral. Enough resin was added to the nucleotide solution so that the pH was lowered to less than 4. Resin was removed by filtration and nucleotide was recovered by evaporation and suspension in dH_2O to a desirable concentration. Final

concentration was determined spectrophotometrically at absorbances appropriate to the specific nucleotide between 260 and 270 nm.

HPLC Analysis of Nucleotides

Using a Waters 1525 dual pump HPLC (Breeze System software), a gradient using solvent A as water and solvent B as 0.8 M ammonium bicarbonate was run at a flow rate of 2 mL/min with the following setup: 0 min, 100 % A, 0 % B; 20 min, 0 % A, 100% B. The column was a PRP-X100 anion exchange (250 mm x 4.6 mm) column (Hamilton). Injections of standard nucleotide solutions (100 nmol nucleotide) were performed to yield peaks for general retention times of each nucleotide. Actual retention times varied based on solvents and ammonium bicarbonate concentration.

LC-MS Analysis of Nucleotides

Samples of an initial concentration of at least 12 mM nucleotide were prepared by addition of acetonitrile to 30 % or methanol to 20 %. Nucleotides in basic solutions were neutralized by addition of 6 M HCl or 1 M phosphate buffer before solvent was included. Samples were analyzed with the assistance of Roland Riesen, Ph.D. using a Bruker Esquire mass spectrometer, under the following electrospray ionization (ESI) conditions: ESI voltage, 4.0 kV; direct infusion; capillary temperature, 300 °C; anion detection; scan range, 50–2200 *m/z*; scan resolution, 0.6 *m/z*.

Synthesis of [^{18}O2]-Uracil

Synthesis of the first isotopically enriched compound, [^{18}O2]-uracil (Steps 1 and 2, Figure 3-1), was performed by Wickliffe Wepukhulu using 97 % + $H_2{}^{18}O$ (Cambridge Isotope Labs) (unpublished work). This compound was verified by LC-MS to ensure proper enrichment of the uracil.

Cloning and Expression of Uracil Phosphoribosyl Transferase (UPRTase) in Parent Plasmid pCAL-n

The *E. coli* UPRTase gene was amplified by PCR from phenol-extracted, genomic DNA using primers designed for insertion into NdeI-HindIII digested pCAL-n vector. The primers (Integrated DNA Technologies) have the following sequences with restriction sites underlined:

5' primer: 5'- AGGTACATATGAAGATCGTGGAAGTCAAA -3'

3' primer: 5'- AGGTAAAGCTTTTATTTCGTACCAAAGATTTT -3'

Amplification reactions were carried out with Vent® DNA polymerase according to the manufacturer's recommendations. Thermal cycles were as follows: one cycle of 94 °C for 5 min, 35 cycles of the following three steps: 94 °C for 30 s, 58 °C for 60 s, 72 °C for 90 s; and a final cycle of 72 °C for a 5 min period. The PCR product was purified, digested with NdeI and HindIII restriction endonucleases, and ligated to NdeI and HindIII-digested pCAL-n with T4 DNA ligase. The recombinant plasmid was then transformed into XL1-Blue cells. Transformation was performed by calcium chloride treatment of XL1-Blue cells, addition of ligation mixture, recovery in LB medium with 2% glucose at 37 °C with shaking and subsequent plating on LB/Amp with 2% glucose plates for growth at 37 °C overnight. Potential plasmids with the desired insert were identified in mini-plasmid preparations from individual colonies arising after the transformation. Several potential positives were further purified and the presence of the insert was verified by restriction digest (as above) and agarose gel electrophoresis. A final transformation (as above) into BL21 cells was performed after verification of the correct insert for the plasmid.

Expression of the UPRTase protein was performed by growth overnight at 37 °C with shaking of the BL21 cells containing the pCAL-UPRTase plasmid in LB/Amp. A secondary culture of LB/Amp was inoculated with a 1:100 dilution of the overnight culture and incubated at 37 °C with shaking for 3 h. Induction for protein production occurred with the addition of IPTG to a final concentration of 50 μM and subsequent growth at 37 °C with shaking for 6 h. The cells were harvested by centrifugation and then resuspended in 800 μL per 50 mL of original cell culture of a buffered solution containing 50 mM Tris-HCl, pH 7.4, 10 % glycerol, 5.0 mM BME, 1.0 mM PMSF, 1 μM pepstatin A and 100 μM leupeptin. The cells were lysed using the Mini Bead Beater with 0.1 mm glass beads using three 1-min pulses at high speed, interspersed with periods of cooling (at least 60 s) the lysate on ice. Centrifugation at 13,000 rpm for 5 min in a microcentrifuge was used to remove cell debris and the assay for crude ACMSD activity was made. Protein size and solubility was observed by SDS-PAGE.

Utilization of UPRTase for Synthesis of [^{18}O2]-UMP

Initial reaction (1 mL volume) was performed using 1 mg unenriched uracil, 25 mM Tris-HCl, pH 8.6, 5 mM $MgCl_2$, 2 mg BSA, as previously described by Jensen, *et al.* [23]. Reaction was started by addition of 5.5 mg phosphoribosyl pyrophosphate (PRPP) (Fluka) and protein carried out in a 37 °C water bath with shaking. [^{18}O2]-UMP synthesis (Step 3, Figure 3-1) was carried out in the same fashion as described above. Reactions for [^{18}O2]-UMP synthesis were scaled up to a total volume of 6 mL. The conversion of uracil to UMP was monitored by HPLC at 270 nm as described above of reaction times ranging between 0 and 80 min. The retention times for uracil and UMP are 4.8 and 6.4 min, respectively. [^{18}O2]-uracil and [^{18}O2]-UMP retention times were 4.8

and 7.0 min, respectively. Once the conversion to [^{18}O2]-UMP was near completion (>95 % converted), the samples were frozen until purification could be carried out. This was to ensure that the [^{18}O2]-UMP would not be degraded by the crude protein. Purification was performed using anion exchange chromatography as described above. After purification, the [^{18}O2]-UMP was analyzed by LC-MS to ensure retention of enrichment.

Syntheses of 5-Br-UMP, 6-cyano-UMP, [^{18}02]-5-Br-UMP, and [^{18}02, ^{13}C-cyano]-6-CN-UMP

Syntheses of 5-Br-UMP and 6-cyano-UMP have been described [24, 25] and were carried out according to recommended protocols. Synthesis of the [^{18}O2]-5-Br-UMP was performed without modification to the original protocol (Step 4, Figure 3-1). Synthesis of [^{18}O2, ^{13}C-*cyano*]-6-CN-UMP was performed by substituting unenriched NaCN with 99% enriched Na^{13}CN (Cambridge Isotope Labs) (Step 5, Figure 3-1). All other conditions remained the same. Purification of nucleotides was performed using an anion exchange column as described above. Retention times for 5-Br-UMP, 6-cyano-UMP, [^{18}O2]-5-Br-UMP, and [^{18}O2, ^{13}C-*cyano*]-6-CN-UMP were 9.3, 11.0, 8.3 and 10.8 min, respectively. Both [^{18}O2]-5-Br-UMP and [^{18}O2, ^{13}C-*cyano*]-6-CN-UMP were analyzed by LC-MS to ensure retention of the isotopic enrichment.

Conversion of [^{18}O2, ^{13}C-cyano]-6-CN-UMP to [^{18}O2, ^{13}C-carboxyl]-OMP

Test reactions to ensure that the conversion of 6-cyano-UMP to OMP would occur but ^{18}O would not exchange from O2 were performed prior to this final synthesis step. Conversion of 6-cyano-UMP to OMP was observed by HPLC (as above) in 0.2 M and 0.5 M NaOH at room temperature and mixed by rocking platform. This reaction

occurs where the formation of an intermediate (UMP-6-carboxamide) can be detected and isolated by HPLC. Retention times for 6-cyano-UMP, UMP-6-carboxamide and OMP were 11.1, 6.4 and 7.6 min, respectively. Approximately 1 mg of [^{18}O2]-uracil was placed in solutions containing a final concentration of either 0.2 or 0.5 M NaOH and mixed by rocking platform at room temperature for up to 8 days. Samples were periodically taken and analyzed by LC-MS to observe whether an exchange of oxygen could be seen at either concentration, as indicated by conversion of the molecular weight of 114 (for [^{18}O2]-uracil) to 112 (for natural abundance).

Reaction of [^{18}O2, ^{13}C-*cyano*]-6-CN-UMP to [^{18}O2, ^{13}C-*carboxyl*]-OMP was performed by placing nucleotide is a solution with a final concentration of 0.5 M NaOH and mixed by rocking platform at room temperature for 4 days (Step 6, Figure 3-1). The reaction was monitored by HPLC until conversion to [^{18}O2, ^{13}C-*carboxyl*]-OMP was over 97 % complete. Retention times of [^{18}O2, ^{13}C-*cyano*]-6-CN-UMP, [^{18}O2, ^{13}C-*carboxamido*]-6-CONH$_2$-UMP, and [^{18}O2, ^{13}C-*carboxyl*]-OMP were 10.8, 6.6 and 7.2 min, respectively. Purification was not considered necessary as no other product is formed in this reaction. Nucleotide was desalted and evaporated as described in the purification of nucleotides section. [^{18}O2, ^{13}C-*carboxyl*]-OMP was analyzed by LC-MS to ensure retention of the enriched elements.

ODCase Assays for CO_2 Collection and Distillation

Reactions for CO_2 collection and distillation were performed in flasks designed to protect samples from interfering atmospheric carbon dioxide. Buffer and substrate were degassed for 15 min with Drierite-scrubbed N_2 before enzyme was added. The enzyme was not degassed because only a small volume would be added to the reaction mix.

Partial reactions were performed first at pH 7.0 in solutions containing a final concentration of 50 mM MOPS, 5 mM OMP, and enzyme. Reaction was initiated by addition of enzyme in an amount sufficient to convert 10 to 20 % of the OMP to UMP in 5 or 6 min. Reactions were performed in a 25 °C water bath to maintain a constant temperature for reaction to occur. Complete conversion reactions were carried out in similar fashion, but twice as much enzyme was added and the reaction was carried out for at least 30 min to ensure completion of the reaction. A second set of partial reactions were performed at pH 5.4 using solutions that contained 50 mM MES, 5 mM OMP, and enzyme. Reactions were carried out in the same manner as described above. For every partial reaction that was performed, a complete reaction was performed in efforts to maintain consistent isotope effect data.

Collection of CO_2 was performed using a specially designed glass distillation system under vacuum. The method of distillation is maintained within our lab.

Isotope Ratio Mass Spectrometer Analysis of Collected CO_2 and Determination of the ^{13}C Kinetic Isotope Effect

Analysis of carbon dioxide collected from distillation was performed using a GV dual inlet Isotope Ratio Mass Spectrometer. Samples were analyzed against standard reference carbon dioxide (Praxair). Determinations of deconvoluted delta values were calculated by the IR-MS. ^{13}C kinetic isotope effects were calculated using the following equation:

$$KIE = [\log (1 - f)] \div \{\log [1 - f \times (R_p/R_s)]\}$$

where f = fraction of reaction (between 0.0 and 1.0), R_p = isotope ratio of the product (determined from partial reaction) and R_s = isotope ratio of the substrate (determined

from complete reaction). Delta values given by the mass spectrometer are converted to isotope ratios R_p and R_s, respectively, as follows: $R_p = 1000 + \delta_p$; $R_s = 1000 + \delta_s$.

Results and Conclusions

Wickliffe Wepukhulu initially verified by LC-MS that [^{18}O2]-uracil contained the proper enrichment (data not shown). It was also confirmed to be unaltered in the presence of 0.2 M and 0.5 M NaOH at room temperature for at least 8 days (Figure 3-3 and Appendix D). The uracil appears to have at least 94.8 % enrichment of ^{18}O only at O2 based on MS data.

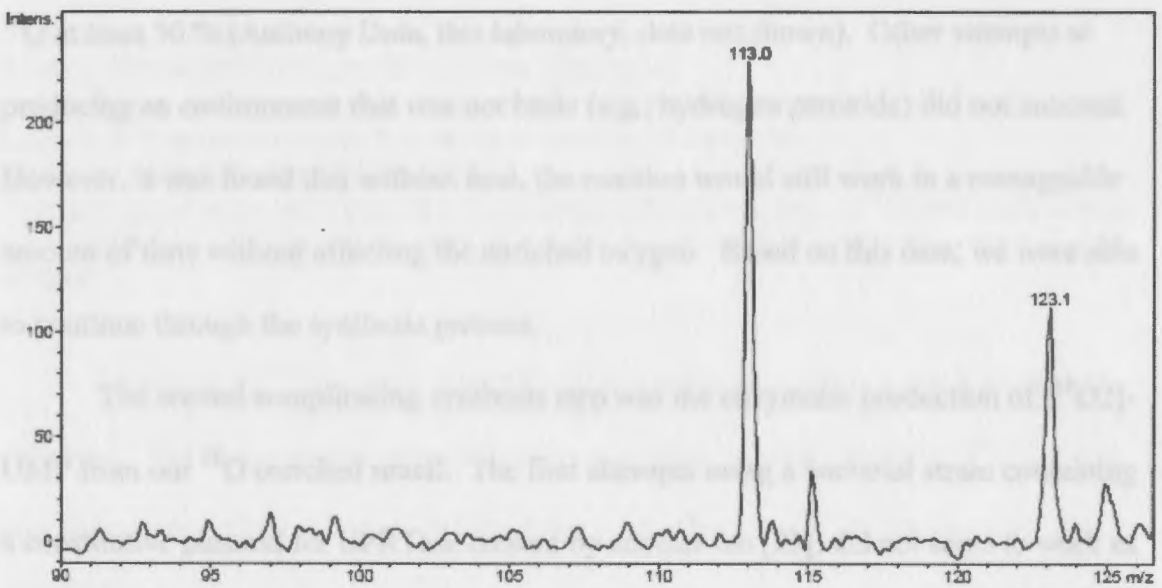

Figure 3-3. MS data of [^{18}O2]-uracil in 0.5 M NaOH after 8 days. The molecular mass of [^{18}O2]-uracil anion is 113 versus the unenriched uracil anion 111.

[^{18}O2]-uracil was used to examine the possibility of oxygen exchange, under conditions necessary for a subsequent step in the synthesis (0.5 M NaOH). This cautionary preliminary test was considered necessary, rather than carrying out the remainder of the synthesis and attempting to observe exchange in one of the nucleotides. Had oxygen

exchange been observed with uracil, it would be necessary to change the synthetic scheme to avoid using the strong base for a reaction. The oxygen exchange should have been quicker with [^{18}O2]-uracil versus the actual starting material [^{18}O2, ^{13}C6-*cyano*]-6-CN-UMP because it is less sterically hindered. The bulkier groups could possibly slow the exchange, which is to our benefit, but no exchange was found to occur with the [^{18}O2]-uracil. The retention of the ^{18}O enrichment at basic conditions was a challenge as previous attempts to maintain the enriched oxygen had not been successful. The suggested synthesis of OMP from 6-cyano-UMP previously [25] included the use of 1 M aqueous base and 100 °C bath for 1 hr. These conditions were found to exchange ^{16}O for ^{18}O at least 50 % (Anthony Dota, this laboratory, data not shown). Other attempts at producing an environment that was not basic (e.g., hydrogen peroxide) did not succeed. However, it was found that without heat, the reaction would still work in a manageable amount of time without affecting the enriched oxygen. Based on this data, we were able to continue through the synthesis process.

The second complicating synthesis step was the enzymatic production of [^{18}O2]-UMP from our ^{18}O enriched uracil. The first attempts using a bacterial strain containing a constitutive plasmid for UPRTase created by another lab [23], did not seem to work as well as originally thought. Cloning of *E. coli* UPRTase was performed in attempts to enhance the activity comparative to the first expression system used. *E. coli* UPRTase is a 627 bp gene and was found to be present after restriction digestion using NdeI and HindIII endonucleases of the cloned pCAL-UPRTase plasmid (data not shown). An induction time course showed the presence of a 22.5 kDa protein after 2 hr and expression of protein was found to be best after 6 hr (Figure 3-4). Because we were only

interested in the activity of the enzyme, the gene was not sequenced and the protein was not purified. However, verification of enzyme activity was enough to attempt synthesis of [^{18}O2]-UMP.

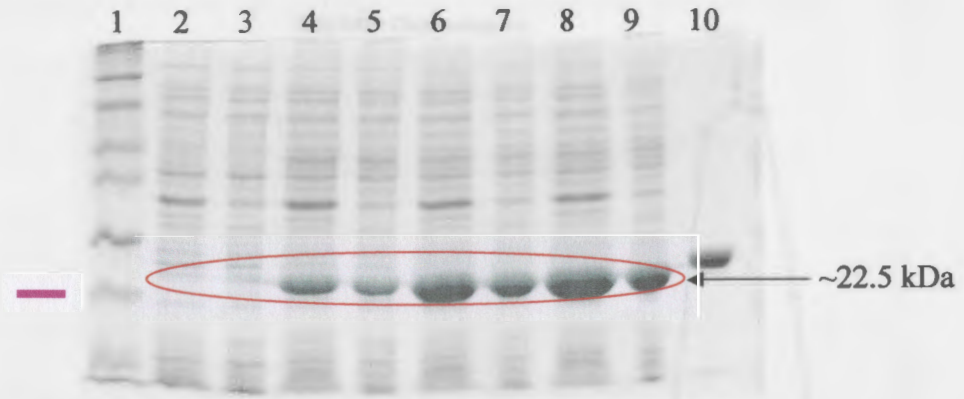

Figure 3-4. SDS-PAGE of Time Course Induction of UPRTase.
Lane 1: Prosieve® color protein markers (Cambrex).
Lanes 2, 4, 6, and 8: 5 μL of 0, 2, 4 and 6 hr whole cells, respectively.
Lane 3, 5, 7 and 9: 10 μg 0, 2, 4 and 6 hr lysates, respectively.
Lane 10: 5 μg of purified ODCase.
The pink band represents the 20 kDa molecular weight marker. UPRTase appearance is circled in red. ODCase was used as a marker to show that it was the correct *E. coli* protein.

Reaction of [^{18}O2]-uracil was difficult due to the solubility of uracil in aqueous solutions. The concentration was difficult to determine so addition of the [^{18}O2]-uracil was done with limited initial solubility of the synthesized uracil. Approximately 10 mg of [^{18}O2]-uracil to 50 mg of PRPP was needed to drive the reaction to completion. This was a costly process and reactions had to be performed with care, as PRPP is an expensive reagent. Reactions to [^{18}O2]-UMP lasted at least 40 min with the longest reaction being 80 min. Samples or reaction mixtures that cannot be purified immediately had to be stored at -20 °C to reduce degradation of the nucleotide. A chromatogram of purification can be seen in Figure 3-5. During the purification process, unconverted [^{18}O2]-uracil was pooled, desalted, and reused to increase the yield of [^{18}O2]-UMP. A

total collection of the pooled [^{18}O2]-UMP was 0.376 mmol. Quantitation of the percent yield is unavailable as the total starting amount is unknown. Other chromatograms, HPLC and MS data can be seen in Appendix E.

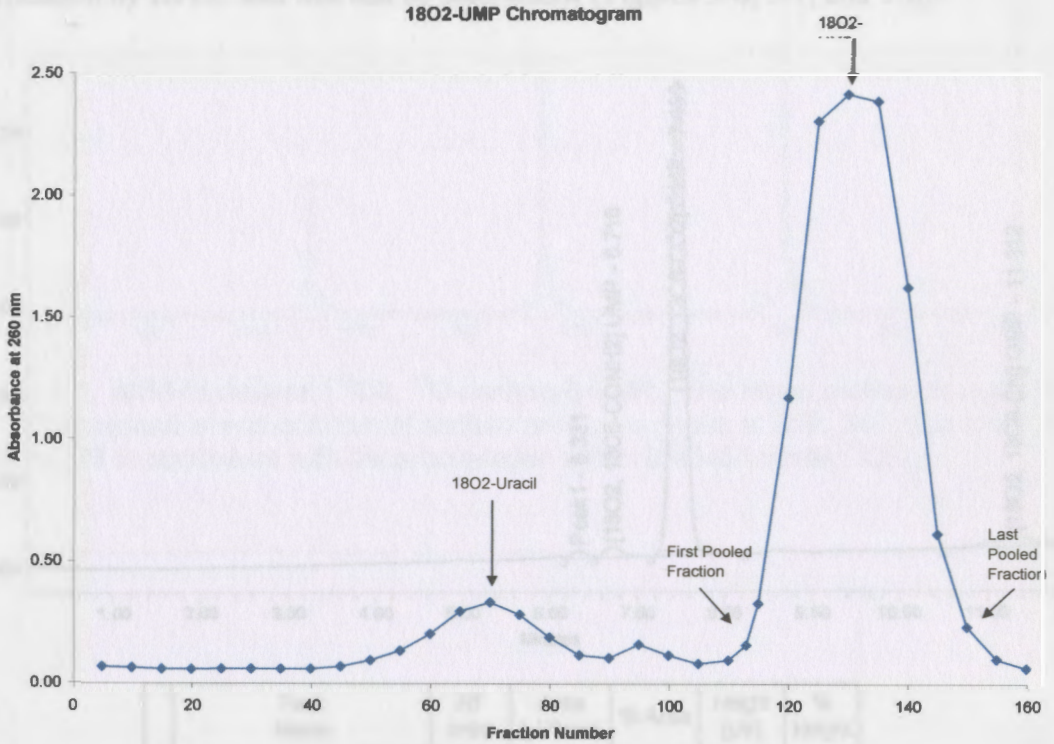

Figure 3-5. Chromatogram of Purification of [^{18}O2]-UMP. UV absorbance was recorded at 260 nm for every five fractions.

Conversion to [^{18}O2]-5-Br-UMP was performed according to protocols set. 0.149 mmol [^{18}O2]-5-Br-UMP was recovered after purification. The chromatogram of purification can be seen in Appendix F. HPLC and MS data obtained showed 100 % purity and retention of isotope enrichment also located in Appendix F.

Conversion to the doubly enriched compound produced 0.18 mmol of [^{18}O2, ^{13}C-*cyano*]-6-CN-UMP. A miscalculation as to the total quantity of [^{18}O2]-5-Br-UMP must

have been made, but the amount did not deviate significantly to be a cause for concern. Chromatogram of purification, HPLC and MS data can be found in Appendix G.

0.11 mmol of [^{18}O2, ^{13}C-*carboxyl*]-OMP was made in the final synthesis step. Verification by HPLC and MS can be seen below (Figures 3-6, 3-7, and 3-8).

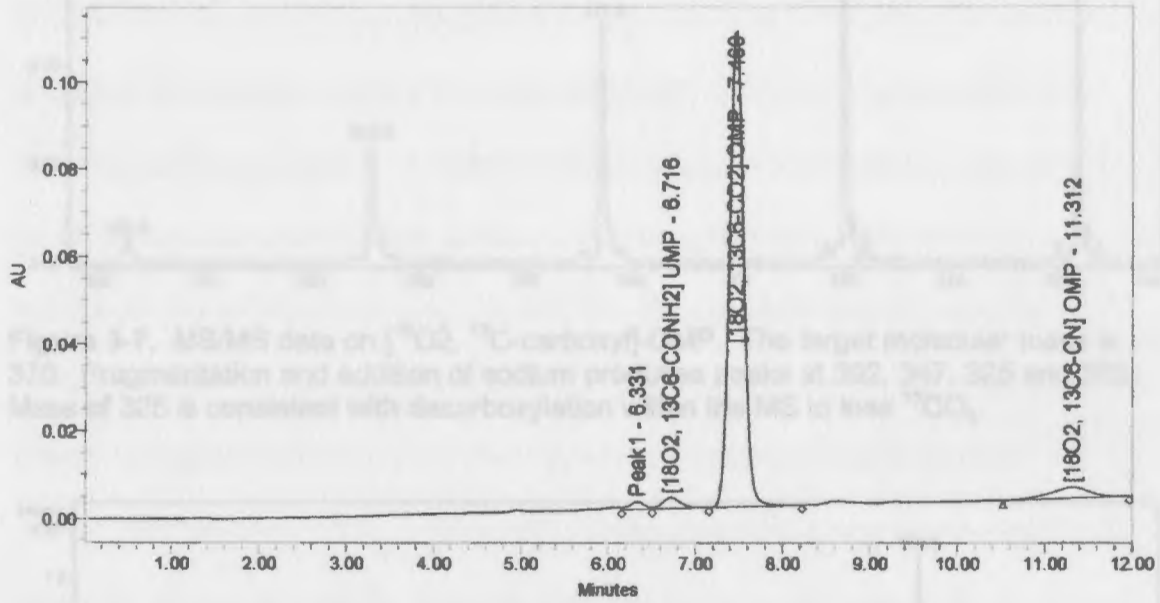

	Peak Name	RT (min)	Area (µV*sec)	% Area	Height (µV)	% Height
1	Peak1	6.331	20461	1.52	1750	1.51
2	[18O2, 13C6-CONH2] UMP	6.716	35973	2.68	2480	2.14
3	[18O2, 13C6-CO2] OMP	7.460	1209486	90.09	108956	94.14
4	[18O2, 13C6-CN] OMP	11.312	76548	5.70	2550	2.20

Figure 3-6. HPLC of [^{18}O2, ^{13}C-*carboxyl*]-OMP in 0.5 M NaOH after 5 days taken at 270 nm. Only 1 µL was used to reduce the quantity used for analysis.

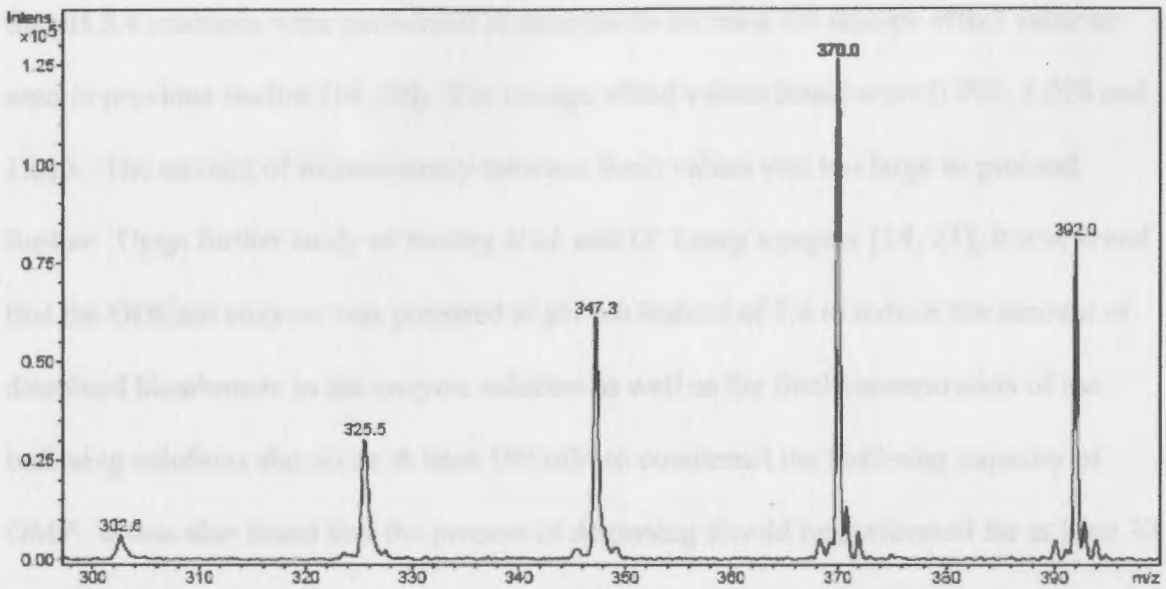

Figure 3-7. MS/MS data on [$^{18}O2$, ^{13}C-*carboxyl*]-OMP. The target molecular mass is 370. Fragmentation and addition of sodium produces peaks at 392, 347, 325 and 303. Mass of 325 is consistent with decarboxylation within the MS to lose $^{12}CO_2$.

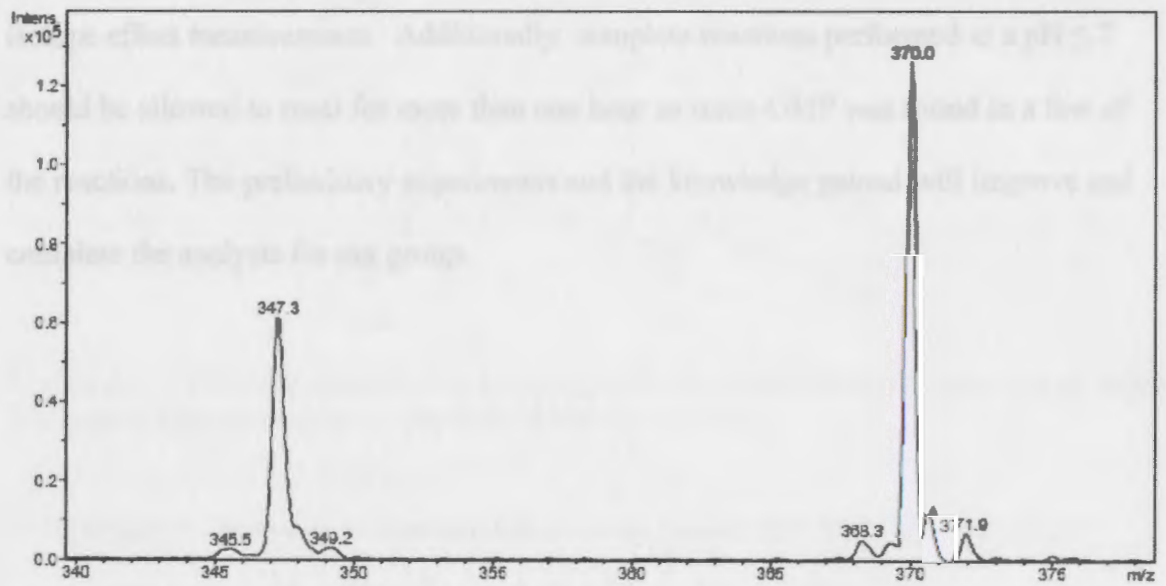

Figure 3-8. Enlargement of Peaks of [$^{18}O2$, ^{13}C-*carboxyl*]-OMP.

The ^{13}C kinetic isotope effect data obtained using the natural abundance OMP with *E. coli* ODCase can be found in Appendix H. The isotope effect measurement values at pH 7.0 were found to be 1.023, 1.017 and 1.027. After trials obtained at pH 7,

the pH 5.4 reactions were performed in attempts to increase the isotope effect value as seen in previous studies [14, 20]. The isotope effect values found were 0.990, 1.028 and 1.013. The amount of inconsistency between these values was too large to proceed further. Upon further study of Smiley *et al.* and O' Leary's papers [14, 21], it was found that the ODCase enzyme was prepared at pH 6.0 instead of 7.4 to reduce the amount of dissolved bicarbonate in the enzyme solution as well as the final concentration of the buffering solutions should be at least 100 mM to counteract the buffering capacity of OMP. It was also found that the process of degassing should be performed for at least 30 min for pH 6.0 solutions and longer for pH 7.0. This indicates that the reactions performed at pH 7.0 (including all complete reactions) contained a significant amount of contaminating atmospheric carbon dioxide, which would significantly decrease the isotope effect measurements. Additionally, complete reactions performed at a pH $\leq$ 7 should be allowed to react for more than one hour as some OMP was found in a few of the reactions. The preliminary experiments and the knowledge gained will improve and complete the analysis for our group.

Chapter 4

Final Discussions on ACMSD and ODCase

Discussion of ACMSD Project

Though no actual mechanistic data could be determined on ACMSD directly, our lab indirectly can make some inferences into how the enzyme works. Another decarboxylase enzyme that is studied in our lab is iso-orotate decarboxylase (IDCase). IDCase is an enzyme that can only be found in fungi, which catalyzes the reaction of uracil 5-carboxylate (iso-orotate) to uracil and carbon dioxide. Viewing the two substrates side by side shows that they are somewhat similar and thus their reaction mechanisms may be related (Figure 4-1).

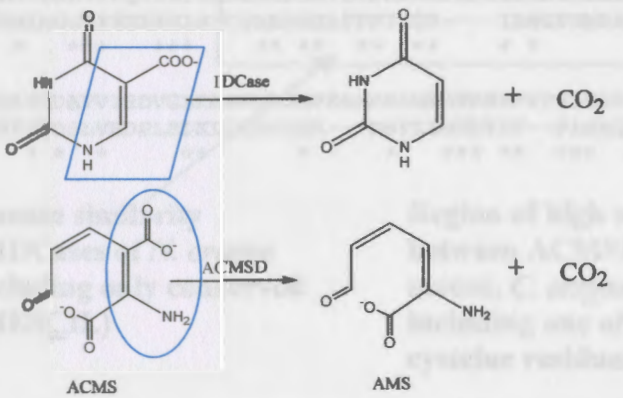

Figure 4-1. Chemical structures of the substrates and products for IDCase and ACMSD. Similarities between the two substrates are circled in blue.

Comparison of the amino acid sequences between IDCase and ACMSD also led our group to investigate the similarities of the two genes (Figure 4-2). It can be seen that the two genes have almost 50% identity. Originally it was thought that both enzymes utilized a cysteine residue to act as a nucleophile and assist decarboxylation. Two cysteine residues were identified in both enzymes for mutagenesis experiments. Because the ACMSD project was discontinued due to insoluble protein, only IDCase mutants

were tested for activity [26]. It was found that despite mutation of the only conserved cysteine residue (suspected to act as a nucleophile) to alanine; mutant IDCase still retained 50 % of its activity. This suggests that our original hypothesis was incorrect about both ACMSD and IDCase. IDCase has also been compared to other enzymes and it has similarities with amidohydrolases. It is now speculated that both IDCase and ACMSD may use water to perform the Michael addition mechanism proposed.

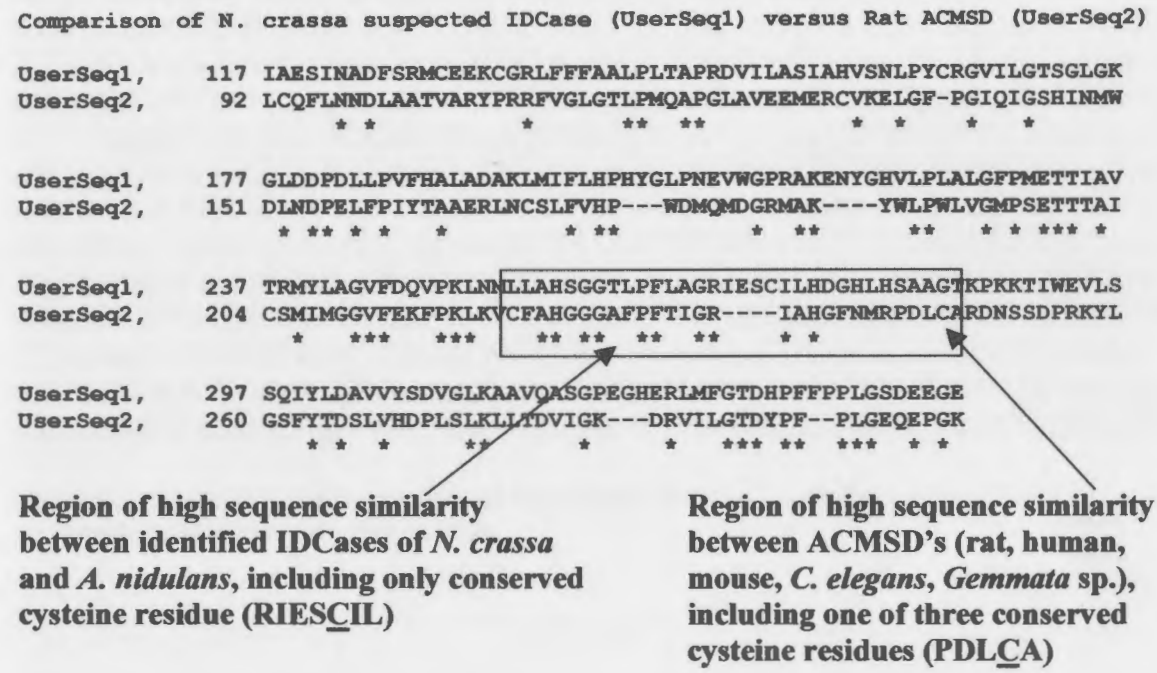

Figure 4-2. Sequence comparison of ACMSD versus IDCase.

Discussion of ODCase Project

Synthesis of the specially enriched compound, [^{18}O2, ^{13}C-*carboxyl*]-OMP proved to be challenging but not impossible. Unfortunately, the isotope effects for ODCase using the isotopically-enriched compound have not been tested by IR-MS, as the process of obtaining purified CO_2 still needs improving. It seems likely that this project will be completed in the near future and results can finally be published as to whether it supports

the protonation mechanism at O2 as is proposed in this thesis or negates this mechanism for the more recognized protonation at C6.

Appendix A

Raw Sequencing Data for Yeast 3-HAO Gene

GNAANNGNTNCNCNCANCCNCNGTTAANAAAATCTCATCCTCCNNTNGGGCA
CTTCTGGTTCCGCGTGGATCCATGTTTAATACTACACCAATTAATATCGACAA
ATGGTTGAAGGAGAACGAAGGCCTTTTGAAACCACCGGTGAATAATTATTGC
TTACATAAAGGGGGATTCACTGTGATGATTGTCGGTGGGCCTAATGAAAGAA
CCGGTTATCACATCAATCCAACTCCCGAATGGTTCTATCAAAAAAAAGGATC
TATGCTTTTAAAGGTTGTGGATGAGACAGACGCTGAACCAAAGTTCATTGAT
ATCATCATCAATGAAGGCGATTCATATTTATTGCCAGGAAATGTTCCTCACAG
TCCTGTTCGGTTTGCTGATACTGTGGGTATTGTTGTGGAACAAGATAGGCCTG
GGGGAGAAAACGATAAGATAAGGTGGTACTGTTCTCATTGTCGCCAAGTGGT
CCACGAGAGTGAACTGCAAATGTTAGACTTAGGTACCCAAGTGAAAGAAGCC
ATTTTAGATTTTGAAAATGATGTCGAAAAGAGGACATGTTTCCATTGCAAGA
CGTTAAACTACGCACGCCCTCAATCTAATTAAGTCGACTCGAGCTCAAGCTTA
GATCCGGCTGCTAACAAAGCCCGAAAGGAAGCTGAGTTGGCTGCTGCCACCG
CTGANCAATAACTAGCATAACCCCTTGGGGGCCTCTAAACGGGGTCTTGAGG
GGGTTTTTNGCTGAAAGGAGGAACTATATNCCGNATATCCCGCAAANAGNNC
CNGGCAGTACCGGNCATANNCCAAGCCNTATNNCCNACAAGCATNCNNGGG
NTGNACNGNTGNCNANAGGNATGACGAAATGAGCCGCANNNGNTNAGANTN
TCANNCNCCGGGNGNCCTGACNGNNNTTANCNATTNAANCNGTGATNNNNN
NNNNNNNAANNNATTCAAANNNNCNGTNCACANNANNNNNTTANACNANNG
GNNNNNGNNNNCNCANTTTTATNGGTANNNTANTNANTATATTGNTTNNNNN

Figure A-1. Underlined in purple are the BamHI and SalI restriction sites. The start and stop codons are bold lettered in blue.

Appendix B

Raw Sequencing Data for Mouse ACMSD Gene

CGAAGNNANTANTNCGGNCNNGNACANAAAANTTNNNCCCNNCTGNNCTNN
CCGGTTCCGCTGGATCCATGAAAATTGACATCCACACTCATATTCTACCAAAG
GAATGGCCCGATCTAGAAAAGAGGTTTGGCTATGGAGGCTGGGTGCAGCTCC
AACAGCAAGGCAAGGGAGAAGCAAAGATGATAAAAGATGGGAAGCTCTTCA
GAGTGATCCAACAGAACTGCTGGGACCCAGAAGTTCGTATCAGAGAAATGAA
CCAGAAAGGAGTGACAGTCCAAGCTCTTTCCACAGTTCCTGTCATGTTTAGCT
ACTGGGCCAAACCTAAGGATACTTTGGAGCTGTGCCAGTTTTTAAACAATGA
CCTAGCTGCCACCGTTGCCAGATACCCTCGAAGGTTTGTGGGTTTGGGGACGT
NGCCTATGCAAGCCCCGGAGCTGGCCGTCGAGGAGATGGAGCGTTGTGTTAA
GGCGCTAGGATTTCCAGGAATCCAGATTGGCTCCCACATCAACACATGGGAC
CTGAATGACCCGGAACCTCTTCCCCAATCTATGCTGCGGCCGAGANGCTGAA
CTGTTNCTCTGTTCGTGCATCCCTGGGATATGCAAATGGATGGACGAATGNNC
NATACTGGCTGCCTTGGGCTCGTAGGAATGCCATCGGAGANCACCANNGCCA
TTTGCTCCATGATCANNGGTGGGGTGTNNGAAAAGTTCCCAAACTCAAAGTG
TGCTTCGCACACCGANGTGGTGCTTTCCCTTCACNATAGGAAAAATTGCCCA
TGGATTCAACATGCNCCCAAATNTCTGTGCCCANGACNANNGTNTGACCCAA
ANNNCCTTGGCCNNTTACACCAACCCCTGTTNACAATCNGTTTCTCAACNATG
ACAATTTTTAGAANGATAANTTTCGGGANNANATACCCTTTCNCNTGGNACA

Figure B-1. Sequencing data obtained using the 5'-end primer for pCAL-ACMSD with the BamHI restriction site. Underlined in purple is the restriction site. The start codon is bold lettered in blue. Italics and bold lettered nucleotides were inserted after raw sequence data was found to differ from the published sequence.

TANNNATTATTATCNTACATTACCTATNATNNGGTATNNNNGGCCNTTGTTNT
CAAATTTGTNANGTTGNCAGNTTATNTTNNATTNGNTTTAATNNGGTAGTTTA
TCACCGGTTTATTGCTAACGCNACGTCCNGGGCACCNGTGTATGANATTTNAC
AATNGCGGTCAATNGTCATCCTNGGCACNNGTCACCCTGGATGCTGTAGGGC
ATAGGCTTGGTTATGCCGGTACTGCCGGGCCTCTTGCGGGATATCCGGATATA
GTTCCTCCTTTCAGCAAAAAACCCCTCAAGACCCGTTTAGAGGGCCCCAAGG
GGTTATGCTAGTTATTGCTCAGCGGTGGCAGCAGCCAACTCAGCTTCCTTTCG
GGCTTTGTTAGCAGCCGGATCTAAGCTTGAGCT***TGA***GTCGACTCATTCAAATA
GTTTTCTCTCAAGACCCAAAAAACGCCAAGGCATTGCCAGCTGTAAGTTTATC
CTTTGTTTCTTCATCAAACTCTGCCATGGACTCTATCAGCTTCCCAGGCTCCTG
CTCGCCCAGAGGAAAGGGGTAATCAGTTCCCAGCATGACTTTATCCTTTCCTA
TGACATCTGTCAATAGCTTGAGAGACAGAGGATCGTGAACCAGGGAGTCTGT
NATAGAAGGAGCCAAGGTANTTTCTGCGGTCGAAGNGAAAAANNNTN

Figure B-2. Sequencing data obtained using the 3'-end primer for pCAL-ACMSD with the SalI restriction site. Underlined in purple is the restriction site. The stop codon is bold lettered in blue. Italics and bold lettered nucleotides were inserted after raw sequence data was found to be missing these nucleotides.

Appendix C

SDS-PAGE gels of ACMSD Expression Conditions

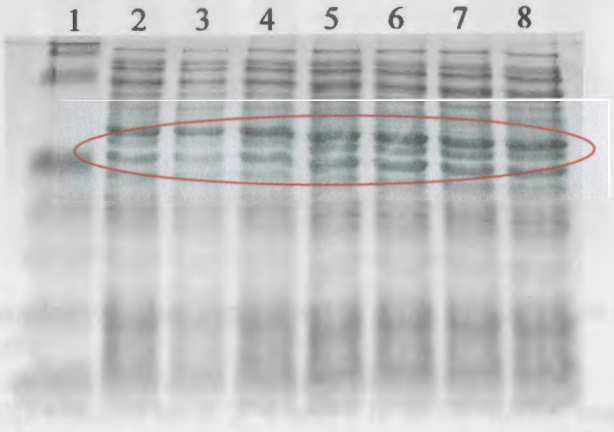

Figure C-1. ACMSD protein lysates expressed at room temperature in LB media.
Lane 1: Kaleidoscope molecular weight markers (Bio-Rad).
Lane 2: 10 µg Lysate under non-inducing conditions.
Lane 3-8: 10 µg ACMSD induced for 2, 4 and 6 hr alternating 0.2 and 0.8 M IPTG final concentrations, respectively. ACMSD should appear in the area circled in red.

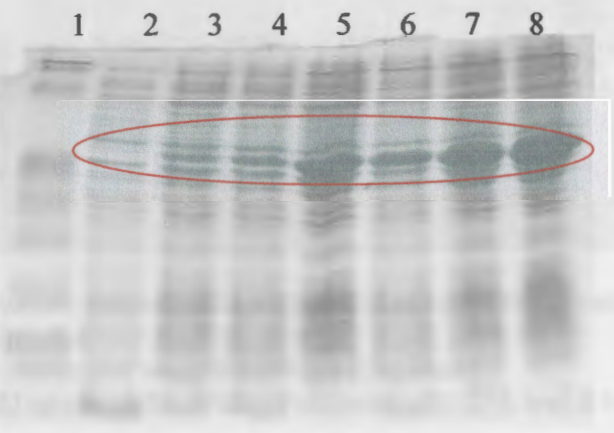

Figure C-2. ACMSD whole cell extracts expressed at room temperature in LB media.
Lane 1: Kaleidoscope molecular weight markers (Bio-Rad).
Lane 2: 10 µL Whole cells under non-inducing conditions.
Lanes 3-8: 10 µL ACMSD whole cell extracts induced for 2, 4 and 6 hr alternating 0.2 and 0.8 M IPTG final concentrations, respectively. ACMSD should appear in the area circled in red.

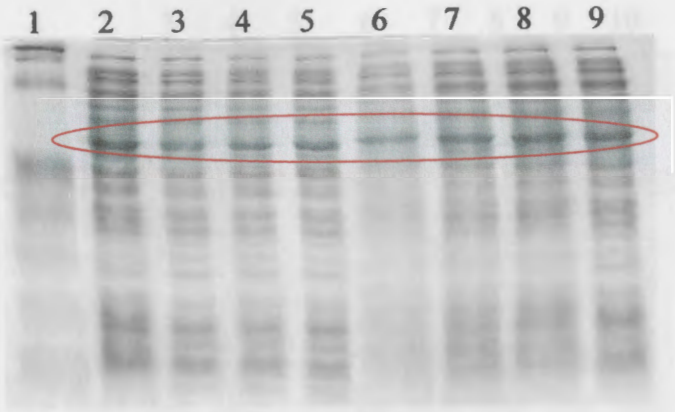

Figure C-3. ACMSD protein lysates expressed at room temperature in LB versus LB plus 10 % glycerol media.
Lane 1: Kaleidoscope molecular weight markers (Bio-Rad).
Lane 2-5: 10 µg ACMSD induced for 0, 2, 4 and 6 hr in LB media, respectively.
Lane 6-9: 10 µg ACMSD induced for 0, 2, 4 and 6 hr in LB plus 10 % glycerol media, respectively. ACMSD should appear in the area circled in red.

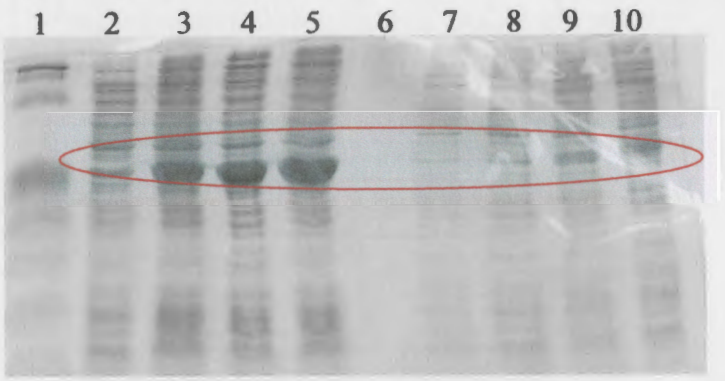

Figure C-4. ACMSD whole cell extracts expressed at room temperature in LB versus LB plus 10 % glycerol media.
Lane 1: Kaleidoscope molecular weight markers (Bio-Rad).
Lane 2-5: 5 µL ACMSD whole cell extracts induced for 0, 2, 4 and 6 hr in LB media, respectively.
Lane 6: Empty.
Lane 7-10: 5 µL ACMSD whole cell extracts induced for 0, 2, 4 and 6 hr in LB plus 10 % glycerol media, respectively. ACMSD should appear in the area circled in red.

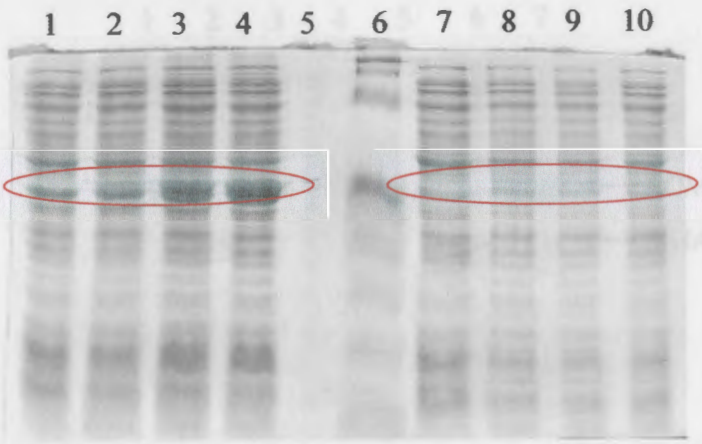

Figure C-5. ACMSD protein expressed at 18 °C in LB media.
Lane 1-4: 5 µL ACMSD whole cell extracts induced for 0, 2, 4 and 6 hr, respectively.
Lane 5: Empty.
Lane 6: Kaleidoscope molecular weight markers (Bio-Rad).
Lane 7-10: 10 µg ACMSD lysates induced for 0, 2, 4 and 6 hr, respectively. ACMSD should appear in the areas circled in red.

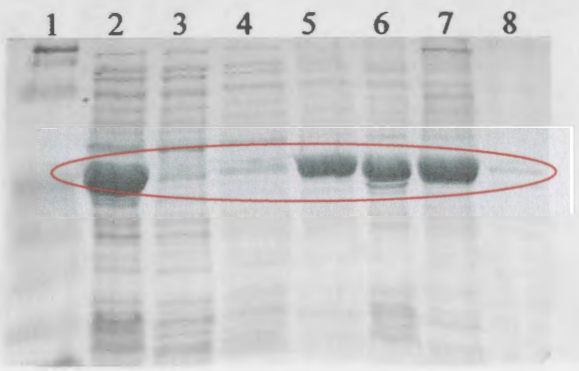

Figure C-6. ACMSD protein induced for 2 hr at 37 °C in LB media and extracted with 8 M urea.
Lane 1: Kaleidoscope molecular weight markers (Bio-Rad).
Lane 2: 5 µL ACMSD whole cell extracts induced for 2 hr.
Lane 3: 10 µg ACMSD lysate induced for 2 hr.
Lane 4: 30 µL of PBS wash after removing lysate.
Lane 5: 3 µL ACMSD supernatant dissolved in 8 M urea.
Lane 6: 5 µL ACMSD pellet in 8 M urea.
Lane 7: Dialysis supernatant of ACMSD in PBS buffer.
Lane 8: Cell pellet after dialysis in PBS buffer. ACMSD should appear in the areas circled in red.

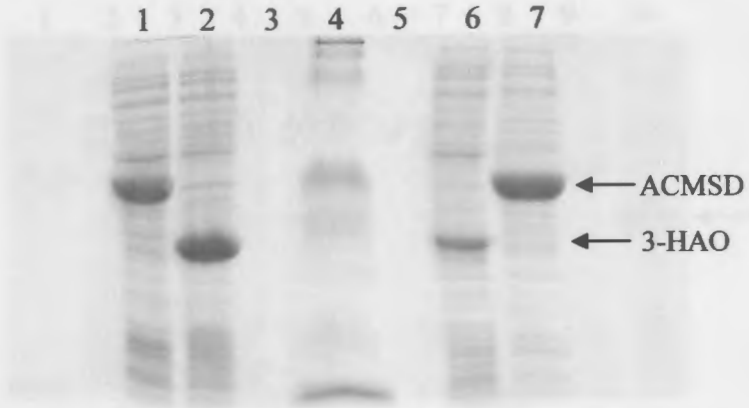

Figure C-7. 3-HAO and ACMSD whole cell extracts and lysates.
Lane 1 and 2: 5 µL for each ACMSD and 3-HAO whole cell extracts, respectively.
Lane 4: Kaleidoscope molecular weight markers (Bio-Rad).
Lane 6: 10 µg 3-HAO crude protein lysate.
Lane 7: 10 µg dialyzed ACMSD supernatant.

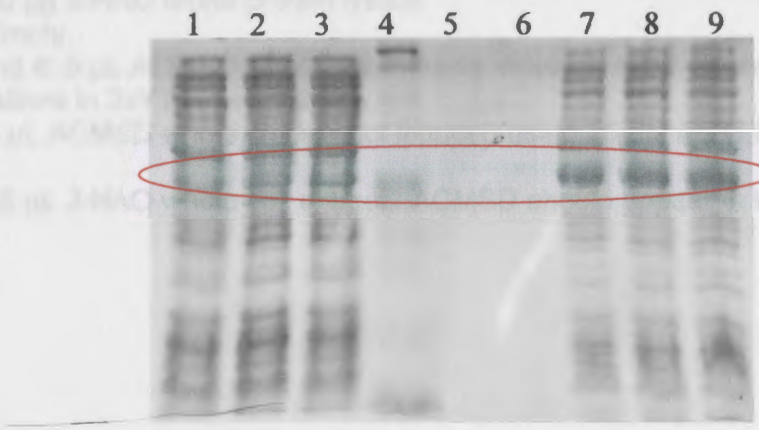

Figure C-8. ACMSD induced using 60-80 µM IPTG final concentrations for 2 hr in 2xYT plus 0.1 % glucose media.
Lane 1-3: 10 µg ACMSD lysates induced using 100, 80 and 60 µM IPTG final concentrations, respectively.
Lane 4: Kaleidoscope molecular weight markers (Bio-Rad).
Lane 5 and 6: Empty.
Lane 7-9: 5 µL ACMSD whole cell extracts 100, 80 and 60 µM IPTG final concentrations, respectively. ACMSD should appear in the area circled in red.

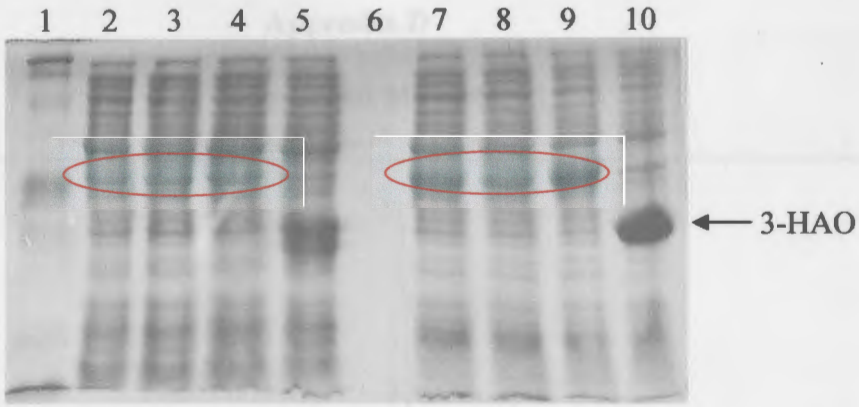

Figure C-9. ACMSD induced using 25-40 µM IPTG final concentrations for 2 hr in 2xYT plus 0.1 % glucose (2xYT/g) media or 25 µM IPTG final concentration for 2 hr in LB media.
Lane 1: Kaleidoscope molecular weight markers (Bio-Rad).
Lane 2 and 3: 10 µg ACMSD lysates induced using 40 and 25 µM IPTG final concentrations in 2xYT/g, respectively.
Lane 4: 10 µg ACMSD lysates induced using 25 µM IPTG final concentration in LB.
Lane 5: 10 µg 3-HAO crude protein lysate.
Lane 6: Empty.
Lane 7 and 8: 5 µL ACMSD whole cell extracts induced using 40 and 25 µM IPTG final concentrations in 2xYT/g, respectively.
Lane 9: 5 µL ACMSD whole cell extract induced using 25 µM IPTG final concentration in LB.
Lane 10: 5 µL 3-HAO whole cell extract. ACMSD should appear in the areas circled in red.

Appendix D

[^{18}O2]-Uracil MS data

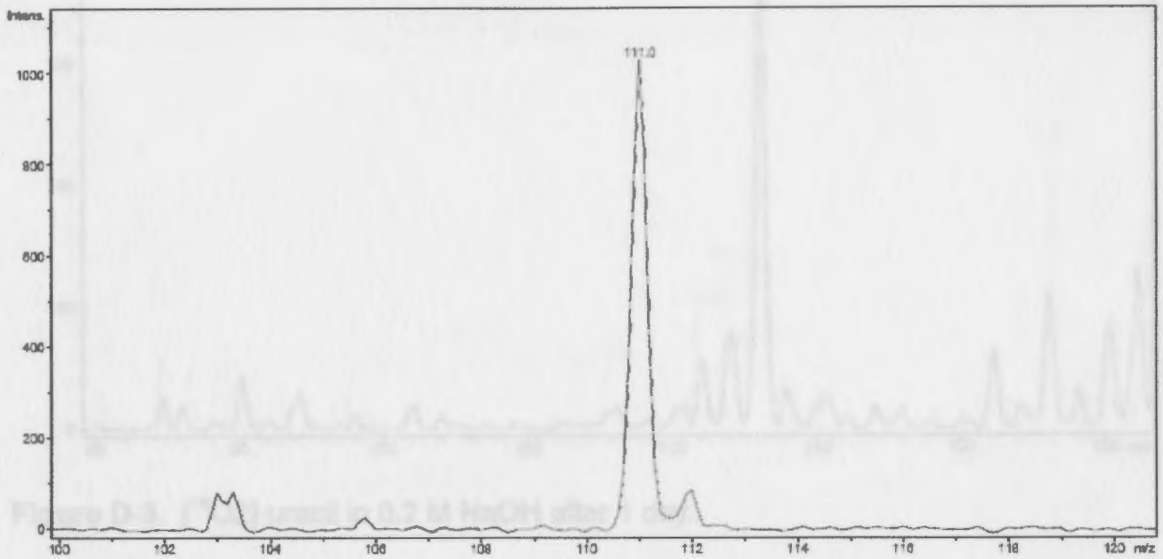

Figure D-1. Unenriched uracil in 0.5 M NaOH. Molecular mass of uracil anion is 111.

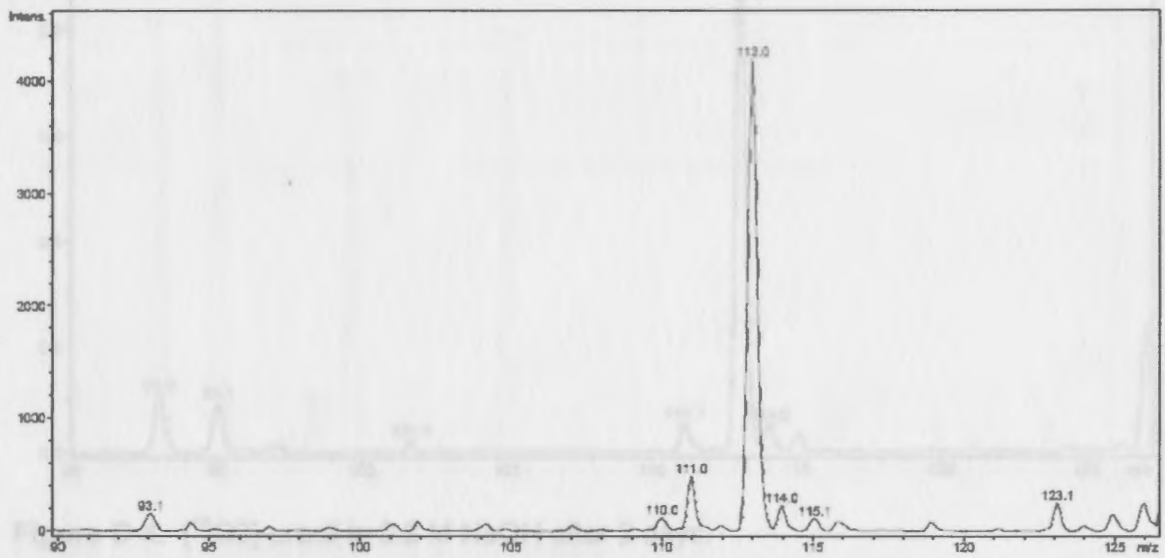

Figure D-2. [^{18}O2]-uracil in 0.2 M NaOH initial data. Molecular mass of the enriched uracil anion is 113 versus the unenriched at 111.

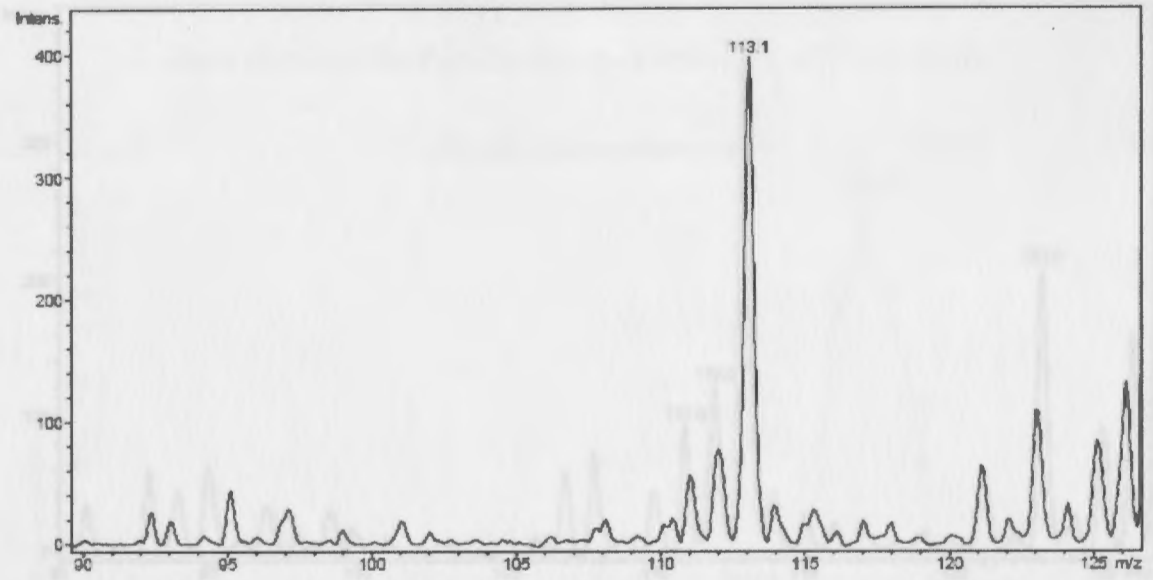

Figure D-3. [^{18}O2]-uracil in 0.2 M NaOH after 1 day.

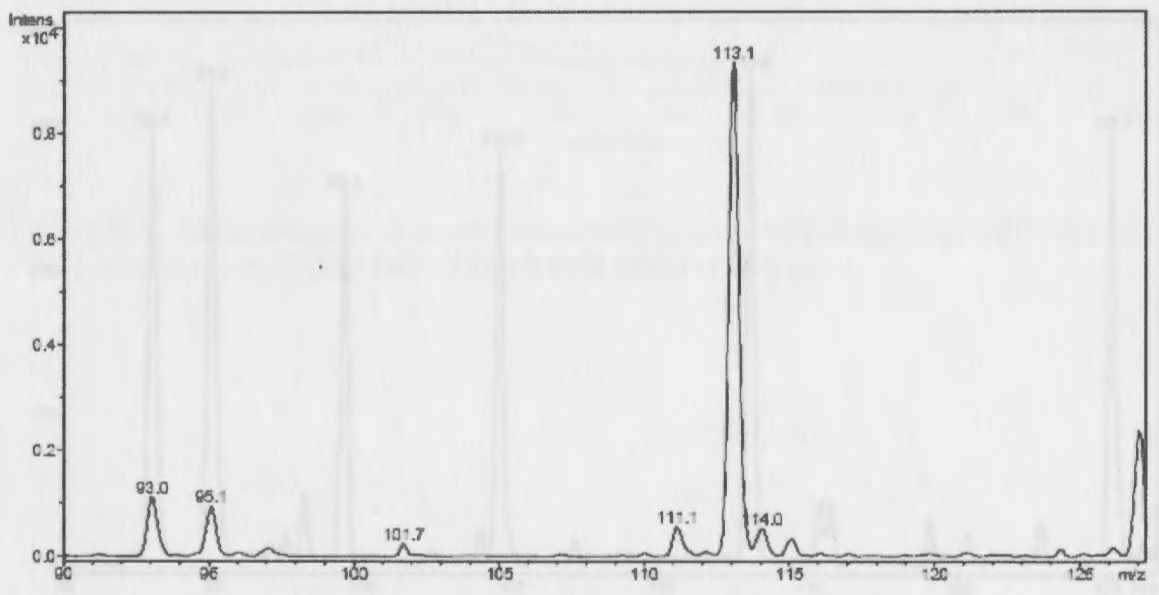

Figure D-4. [^{18}O2]-uracil in 0.2 M NaOH after 2 days.

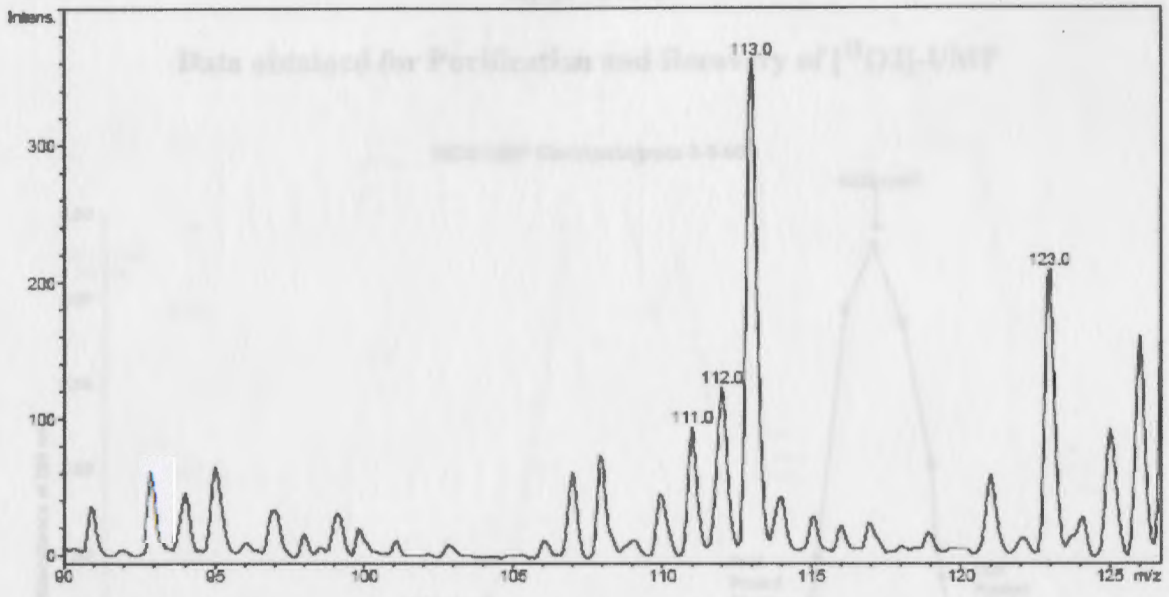

Figure D-5. [^{18}O2]-uracil in 0.5 M NaOH after 1 day.

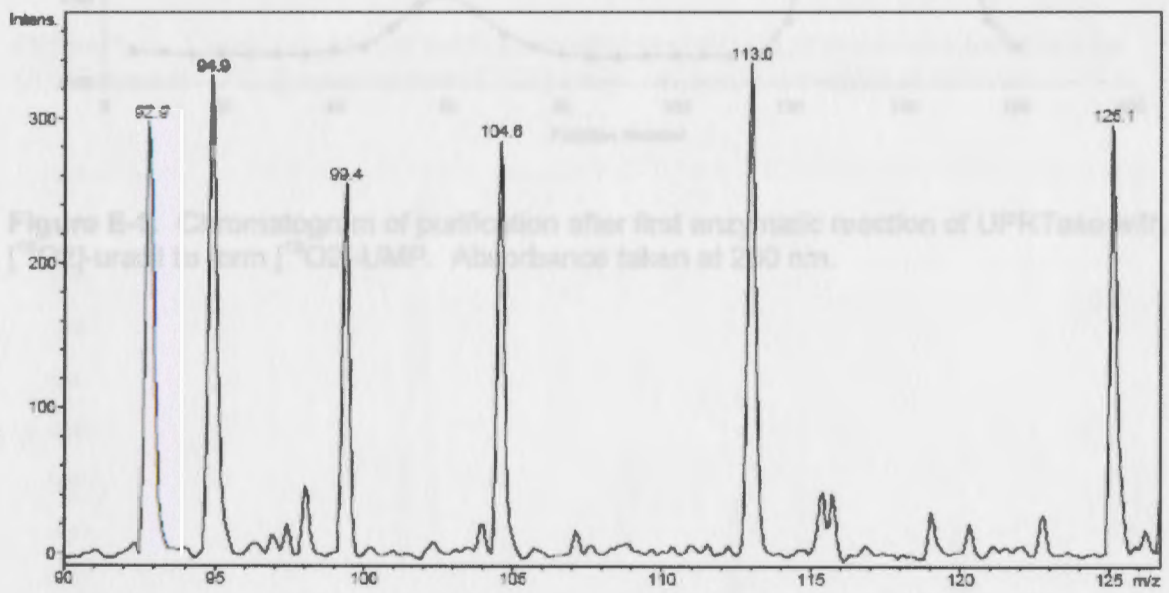

Figure D-6. [^{18}O2]-uracil in 0.5 M NaOH after 2 days.

Appendix E

Data obtained for Purification and Recovery of [^{18}O2]-UMP

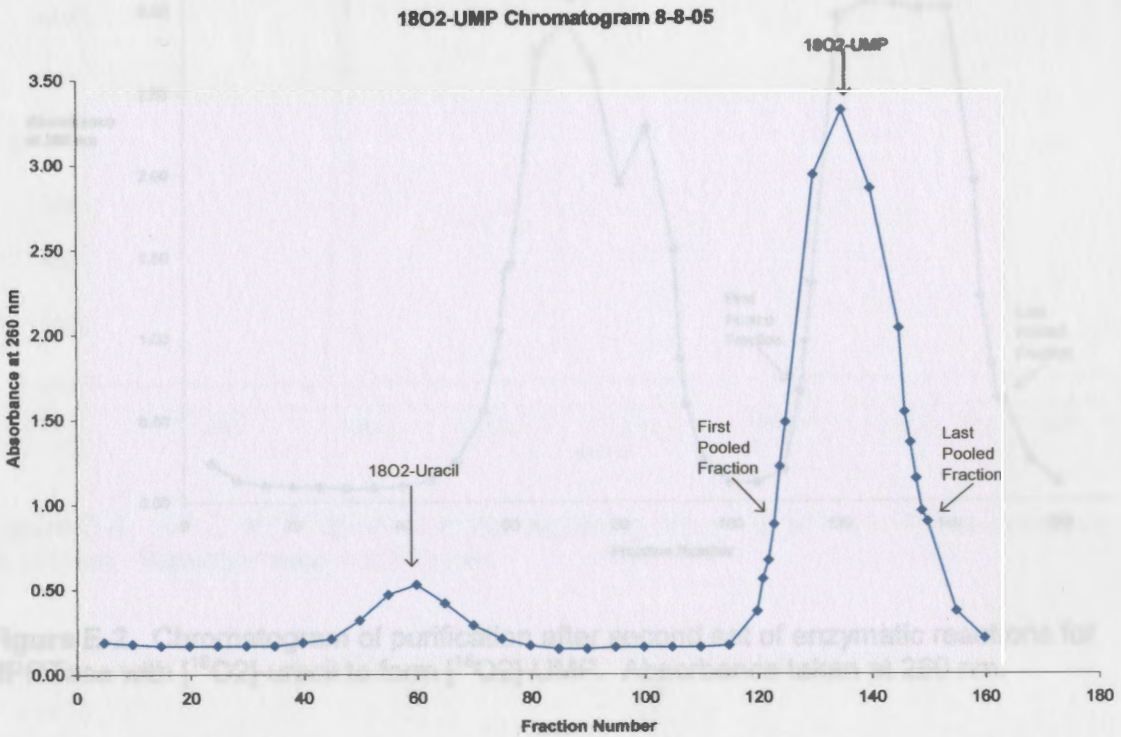

Figure E-1. Chromatogram of purification after first enzymatic reaction of UPRTase with [^{18}O2]-uracil to form [^{18}O2]-UMP. Absorbance taken at 260 nm.

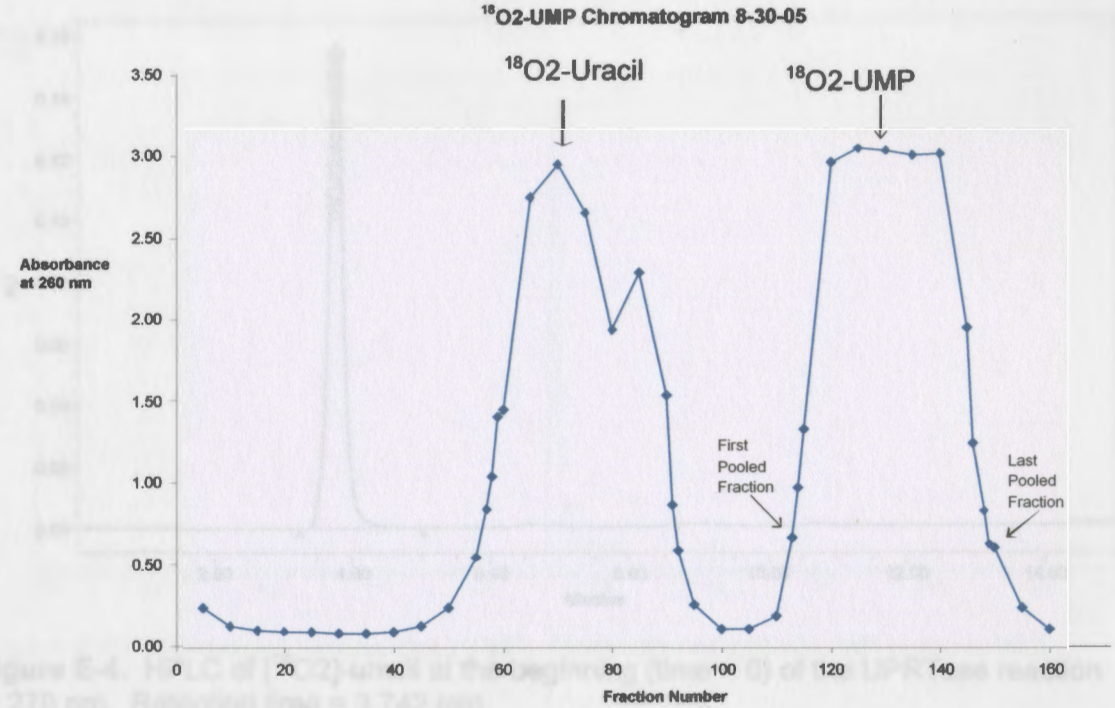

Figure E-2. Chromatogram of purification after second set of enzymatic reactions for UPRTase with [^{18}O2]-uracil to form [^{18}O2]-UMP. Absorbance taken at 260 nm.

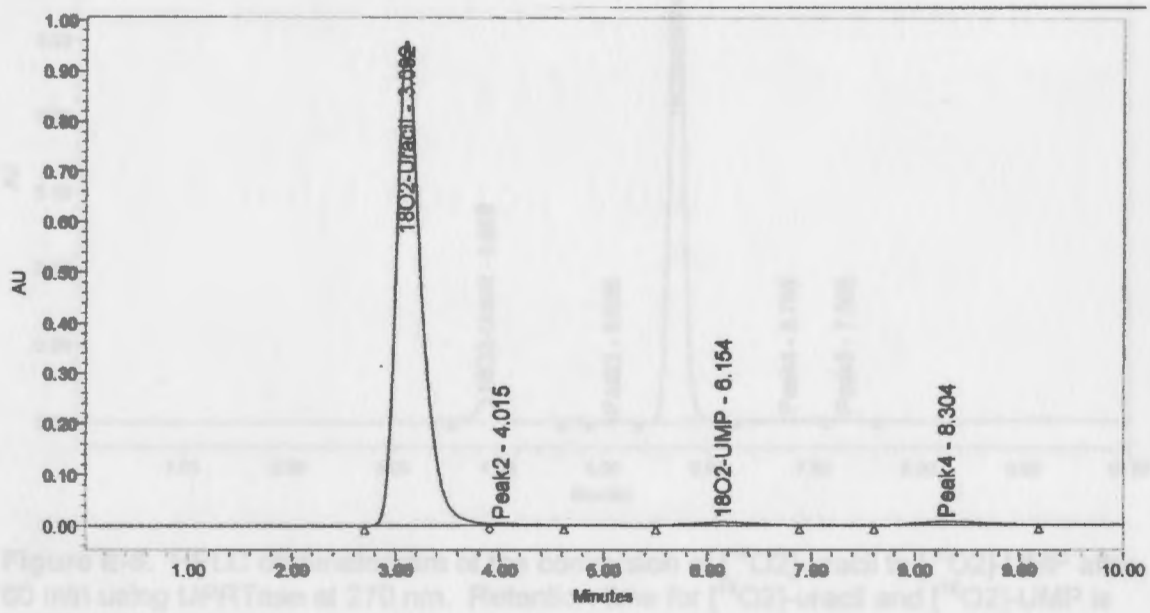

Figure E-3. HPLC Chromatogram at 270 nm for 100 nmol of standard [^{18}O2]-uracil. Retention time = 3.092 min.

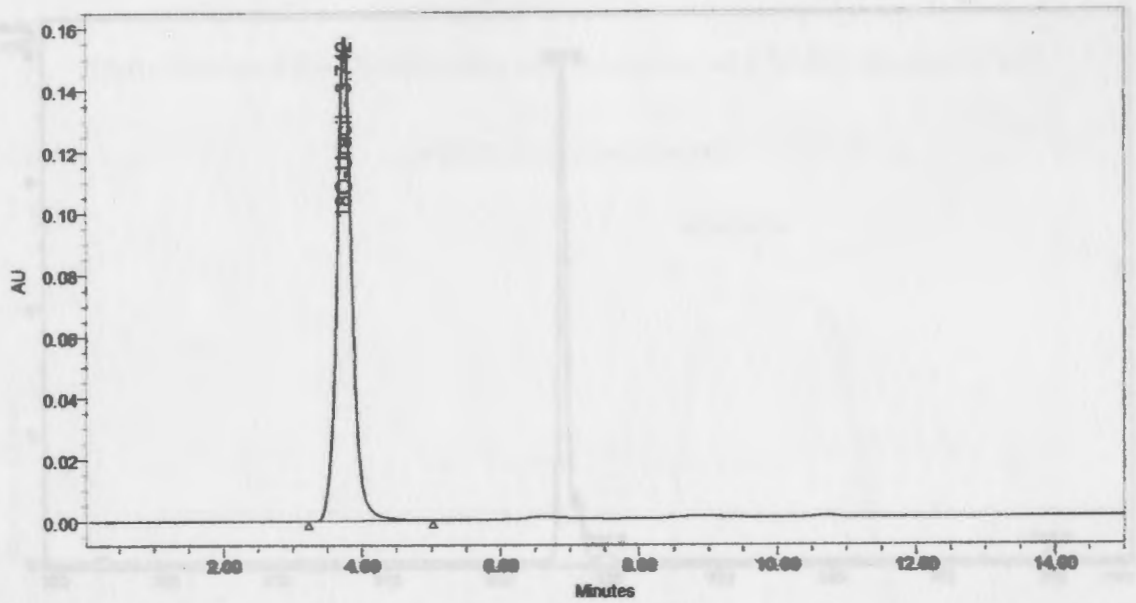

Figure E-4. HPLC of [^{18}O2]-uracil at the beginning (time = 0) of the UPRTase reaction at 270 nm. Retention time = 3.742 min.

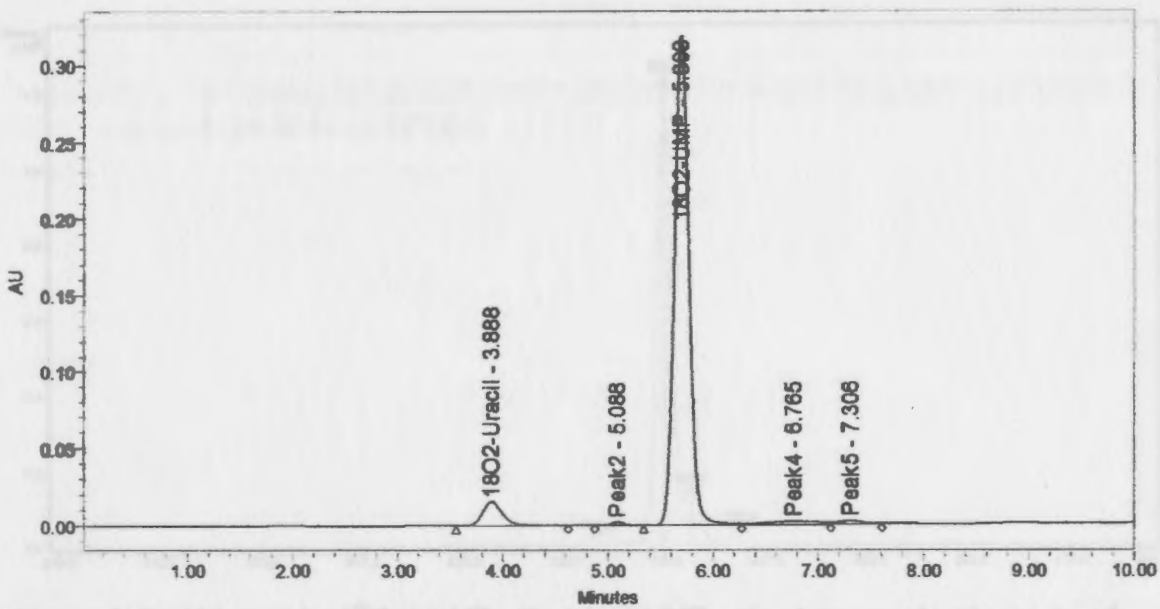

Figure E-5. HPLC chromatogram of the conversion of [^{18}O2]-uracil to [^{18}O2]-UMP after 60 min using UPRTase at 270 nm. Retention time for [^{18}O2]-uracil and [^{18}O2]-UMP is 3.888 and 5.693 min, respectively.

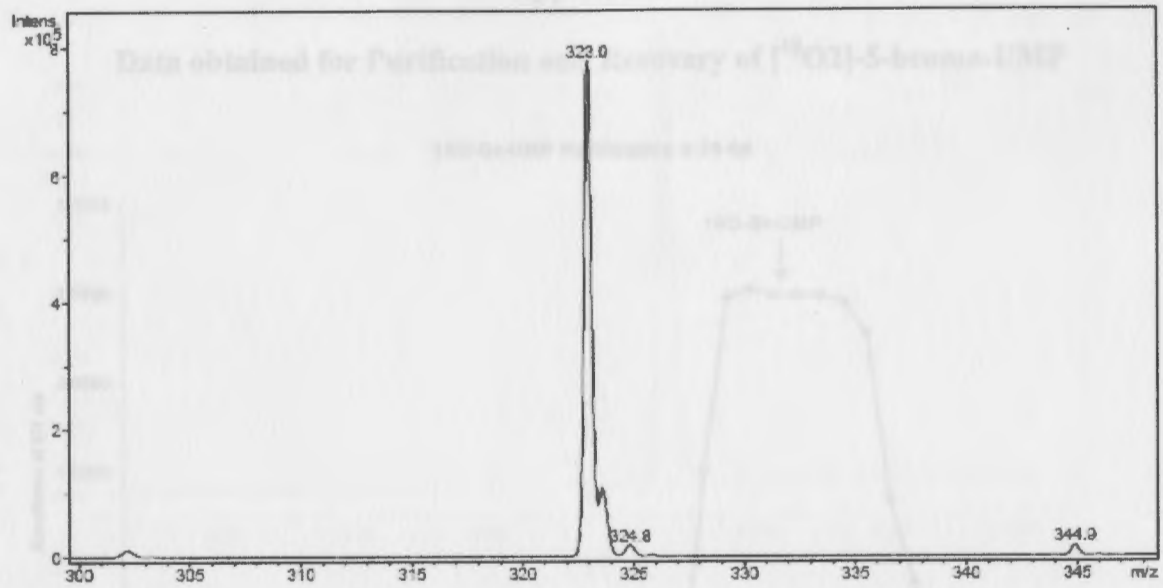

Figure E-6. MS data for unenriched UMP. Molecular weight of UMP anion is 323.

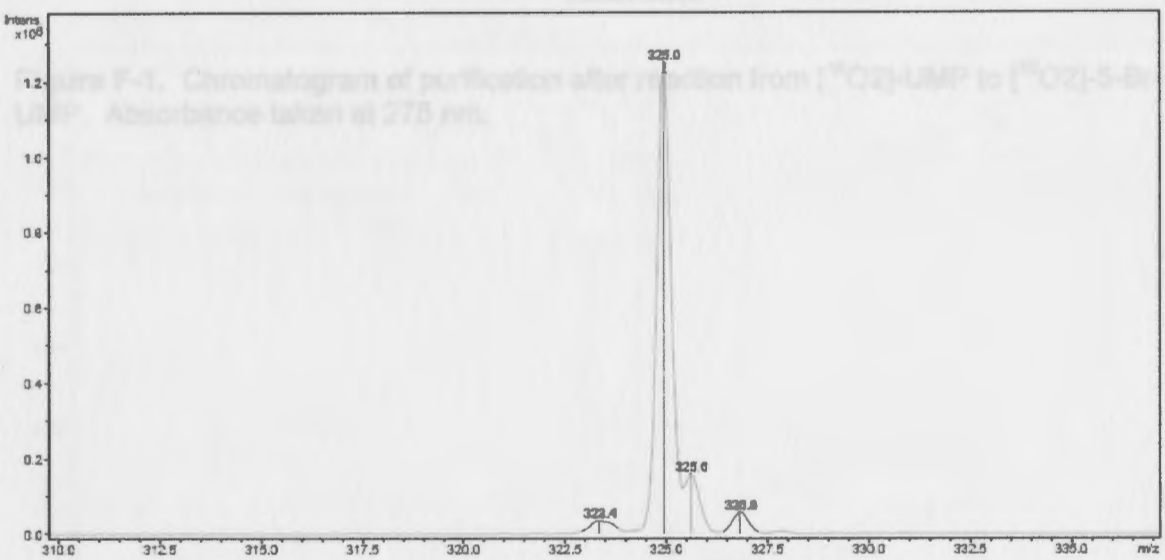

Figure E-7. MS data for [^{18}O2]-UMP. Enriched UMP anion has a molecular mass of 325 versus the unenriched 323.

Appendix F

Data obtained for Purification and Recovery of [^{18}O2]-5-bromo-UMP

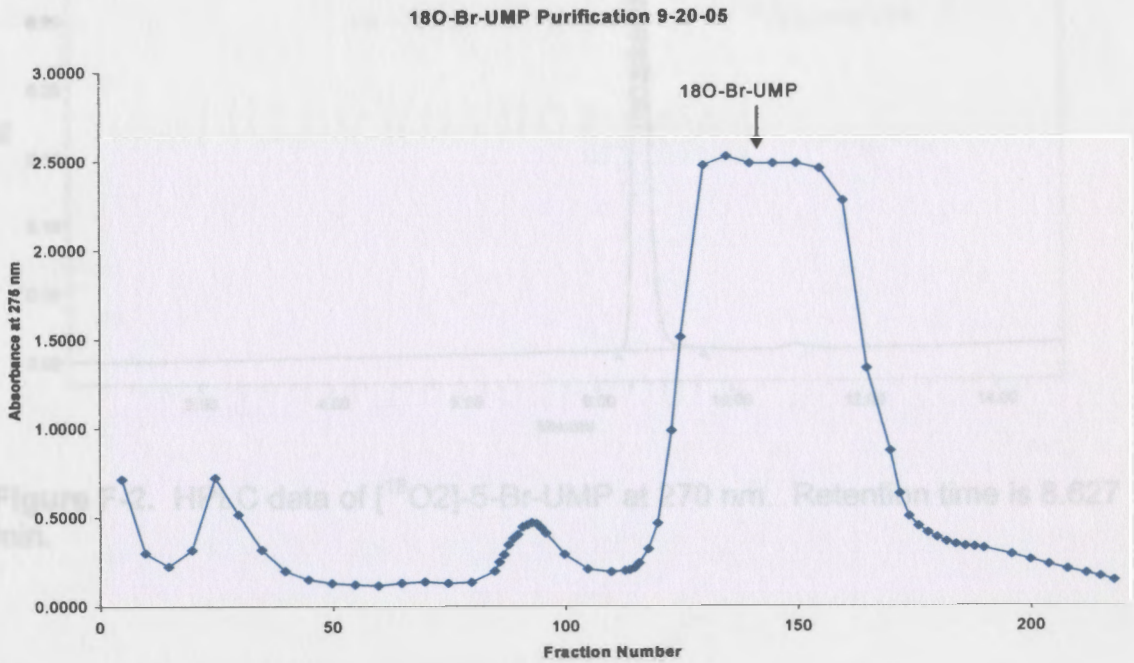

Figure F-1. Chromatogram of purification after reaction from [^{18}O2]-UMP to [^{18}O2]-5-Br-UMP. Absorbance taken at 275 nm.

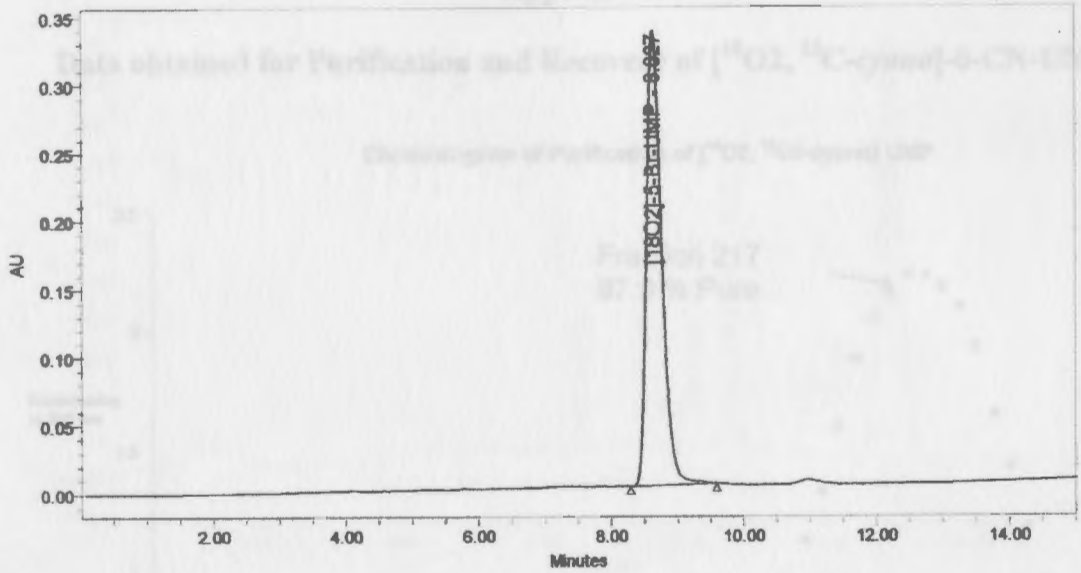

Figure F-2. HPLC data of [^{18}O2]-5-Br-UMP at 270 nm. Retention time is 8.627 min.

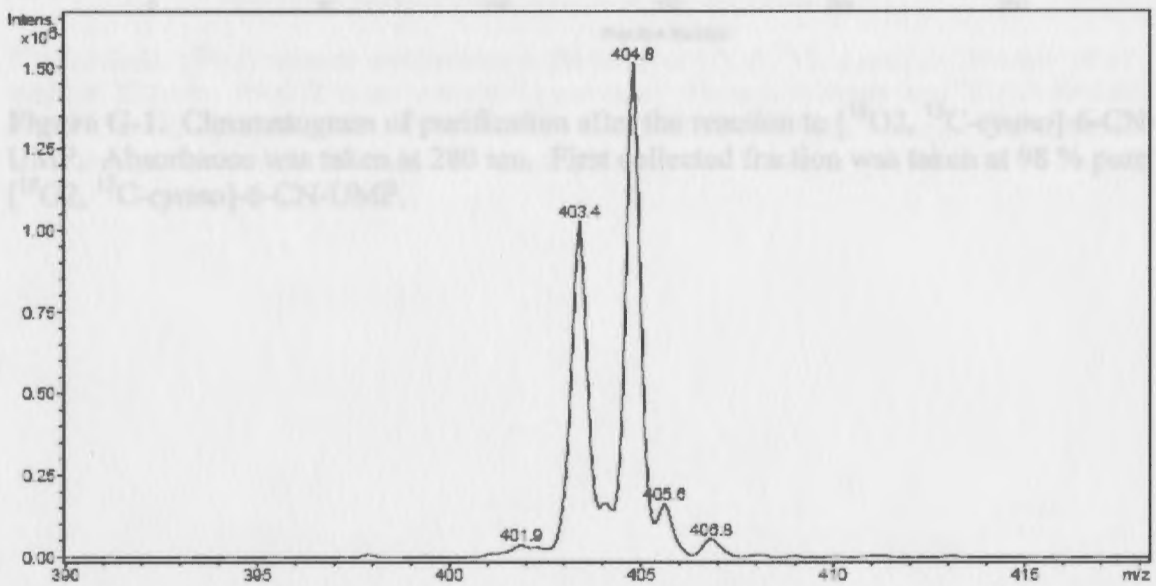

Figure F-3. MS data for [^{18}O2]-5-Br-UMP. Molecular mass of anion is a mixture of 403 and 405.

Appendix G

Data obtained for Purification and Recovery of [^{18}O2, ^{13}C-*cyano*]-6-CN-UMP

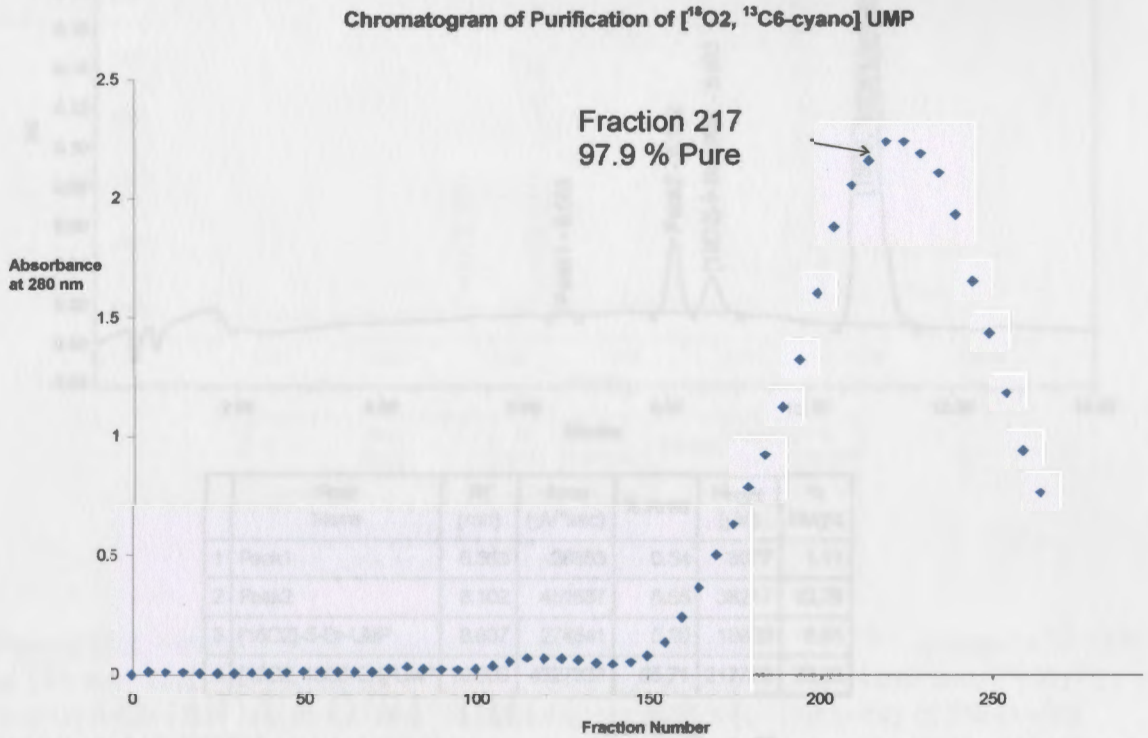

Figure G-1. Chromatogram of purification after the reaction to [^{18}O2, ^{13}C-*cyano*]-6-CN-UMP. Absorbance was taken at 280 nm. First collected fraction was taken at 98 % pure [^{18}O2, ^{13}C-*cyano*]-6-CN-UMP.

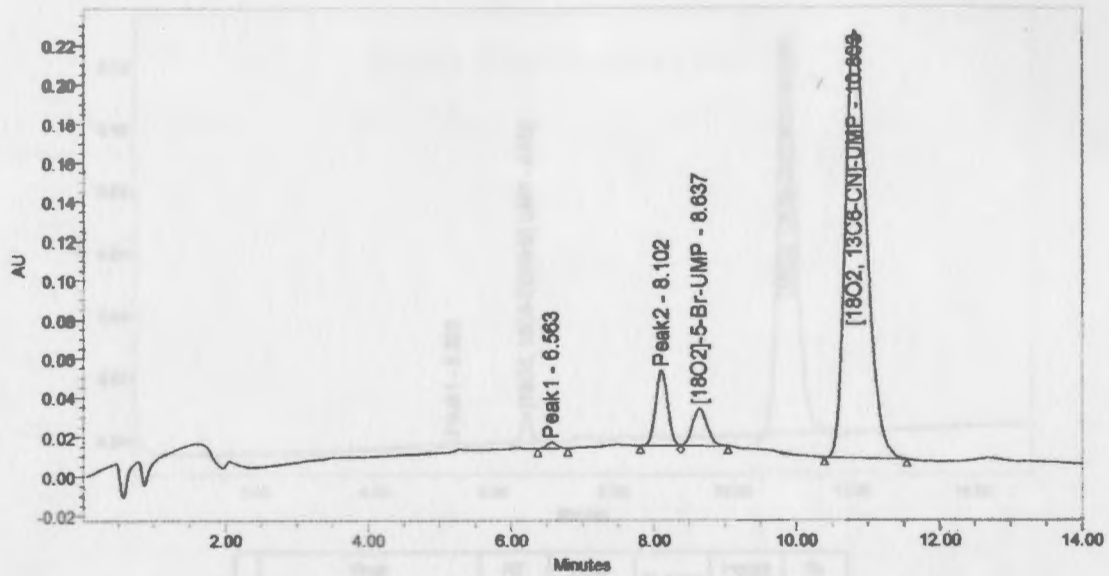

	Peak Name	RT (min)	Area (µV*sec)	% Area	Height (µV)	% Height
1	Peak1	6.563	28653	0.54	3077	1.11
2	Peak2	8.102	451537	8.55	38217	13.75
3	[18O2]-5-Br-UMP	8.637	274641	5.20	18930	6.81
4	[18O2, 13C6-CN]-UMP	10.803	4527333	85.71	217730	78.33

Figure G-2. HPLC data of conversion to 25 nmol of [^{18}O2-^{13}C-*cyano*]-6-CN-UMP after 7 days at 270 nm. Peak 2 is an unknown byproduct. Retention times for [^{18}O2]-5-Br-UMP and [^{18}O2-^{13}C-*cyano*]-6-CN-UMP are 8.637 and 10.803 min, respectively. The reaction was carried out to approximately 86 % completion.

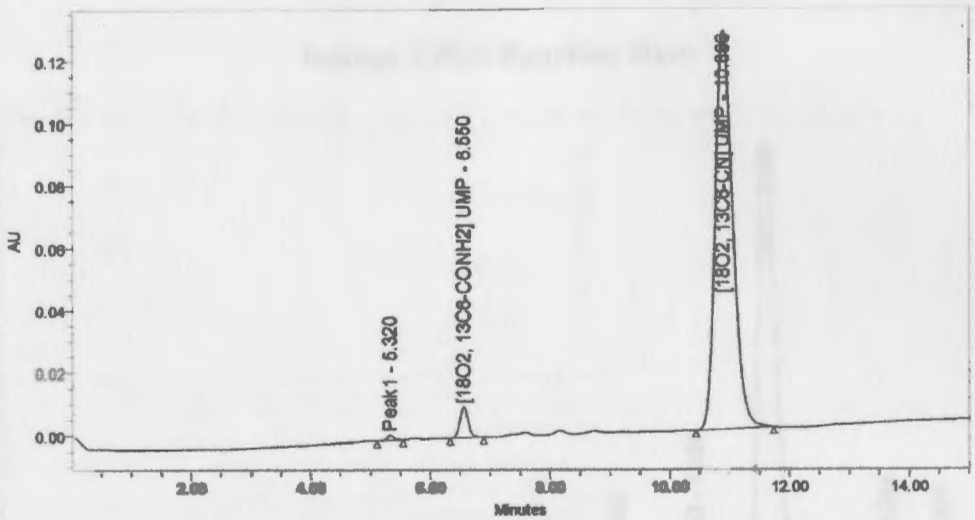

	Peak Name	RT (min)	Area (µV*sec)	% Area	Height (µV)	% Height
1	Peak1	5.320	11683	0.44	1619	1.16
2	[18O2, 13C6-CONH2] UMP	6.550	93202	3.49	9754	7.01
3	[18O2, 13C6-CN] UMP	10.886	2563895	96.07	127828	91.83

Figure G-3. HPLC data of 28 nmol of purified and desalted [^{18}O2-^{13}C-*cyano*]-6-CN-UMP at 270 nm. Retention times for [^{18}O2, ^{13}C-*carboxamido*]-6-CONH$_2$-UMP and [^{18}O2-^{13}C-*cyano*]-6-CN-UMP are 6.550 and 10.886 min, respectively. The purity of the doubly enriched 6-CN-UMP is about 96 %.

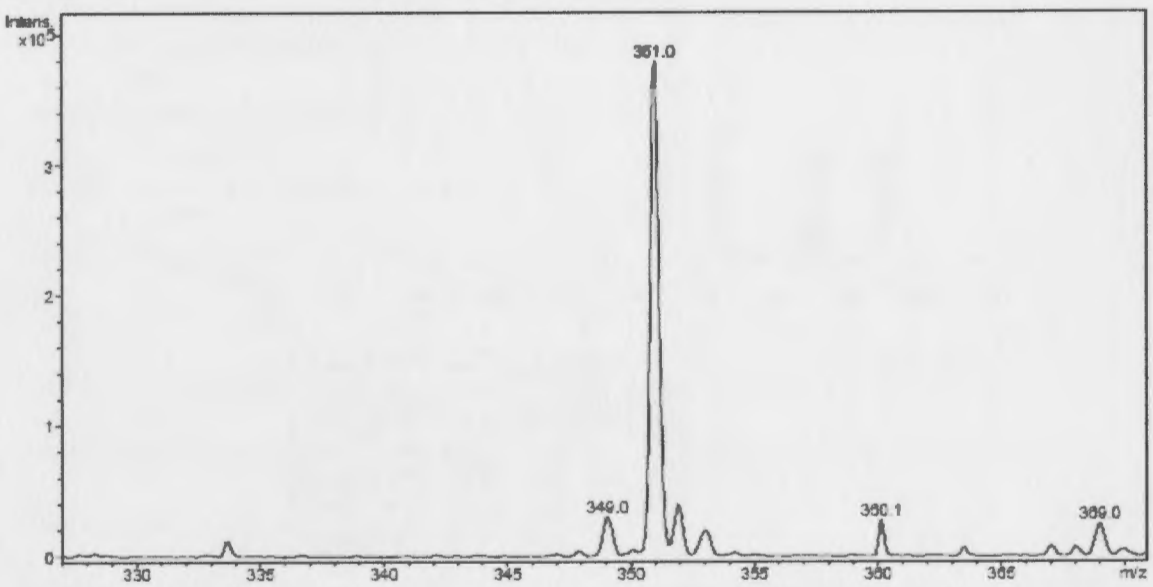

Figure G-4. MS data of [^{18}O2-^{13}C-*cyano*]-6-CN-UMP. Molecular mass of enriched anion is 351.

Appendix H

Isotope Effect Reaction Data

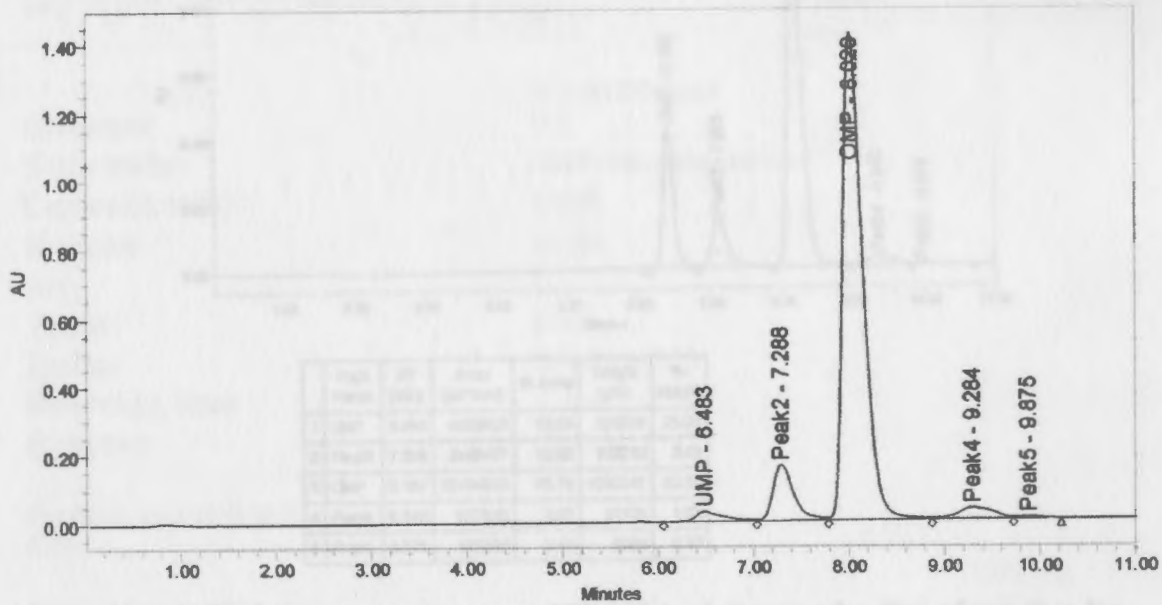

Figure H-1. HPLC data of 100 nmol of the natural abundance OMP used for ODCase reactions at 270 nm. Retention time of OMP is 8.020 min.

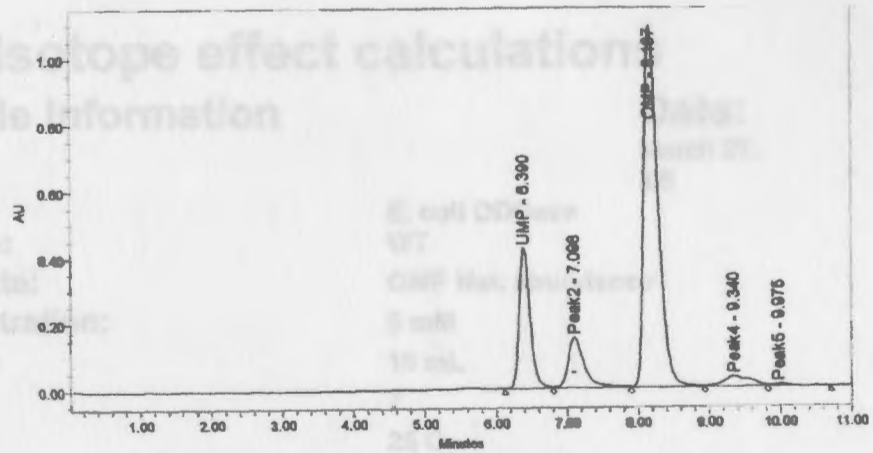

	Peak Name	RT (min)	Area (μV*sec)	% Area	Height (μV)	% Height
1	UMP	6.390	4486806	19.55	426738	25.04
2	Peak2	7.098	2440477	10.63	150212	8.81
3	OMP	8.167	15104980	65.78	1090141	63.97
4	Peak4	9.340	827449	3.60	31125	1.83
5	Peak5	9.975	102019	0.44	6020	0.35

Figure H-2a. HPLC data (absorbance at 270 nm) to determine fraction of reaction for ODCase isotope effect measurement, natural abundance OMP, pH 7.0, trial #1.

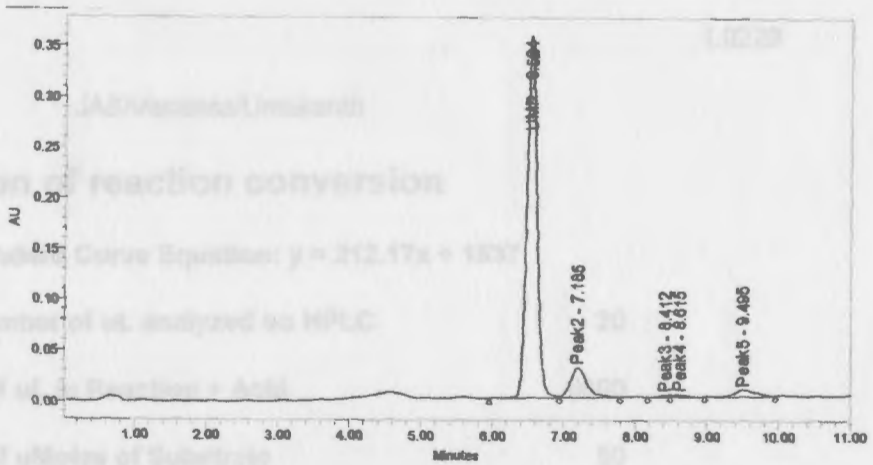

	Peak Name	RT (min)	Area (μV*sec)	% Area	Height (μV)	% Height
1	UMP	6.524	3531319	83.83	357700	89.99
2	Peak2	7.185	472879	11.23	29278	7.37
3	Peak3	8.412	21093	0.50	1902	0.48
4	Peak4	8.615	34323	0.81	2291	0.58
5	Peak5	9.495	152733	3.63	6333	1.59

Figure H-2b. HPLC data (absorbance at 270 nm) to verify complete reaction for ODCase isotope effect measurement, natural abundance OMP, pH 7.0, trial #1.

CO_2 Isotope effect calculations

Sample Information

Date: March 27, '06

Enzyme:	**E. coli ODCase WT**
Substrate:	**OMP Nat. abundance**
Concentration:	**5 mM**
Volume	**10 mL**
pH	**7**
Temp.	**25 C**
Buffer	**50 mM MOPS**
Reaction time	**5 min.**
Enzyme	**83 mg**

Fraction reaction (0.0 - 1.0)	0.135	
		1000 + δ
Delta value (partial rxn)	20.0	1020.0
Delta value (100% conversion)	41.7	1041.7
Isotope effect	1.0229	
User	JAS/Vanessa/Umakanth	

Fraction of reaction conversion

UMP Standard Curve Equation: y = 212.17x + 1537

Enter Number of uL analyzed on HPLC	20
Enter # of uL in Reaction + Acid	9800
Enter # of uMoles of Substrate	50
Enter peak area/1000	4470
nmol in HPLC sample	13.82
Fraction of Reaction	0.135

Table H-2. Isotope ratio data for ODCase isotope effect measurement, natural abundance OMP, pH 7.0, trial #1.

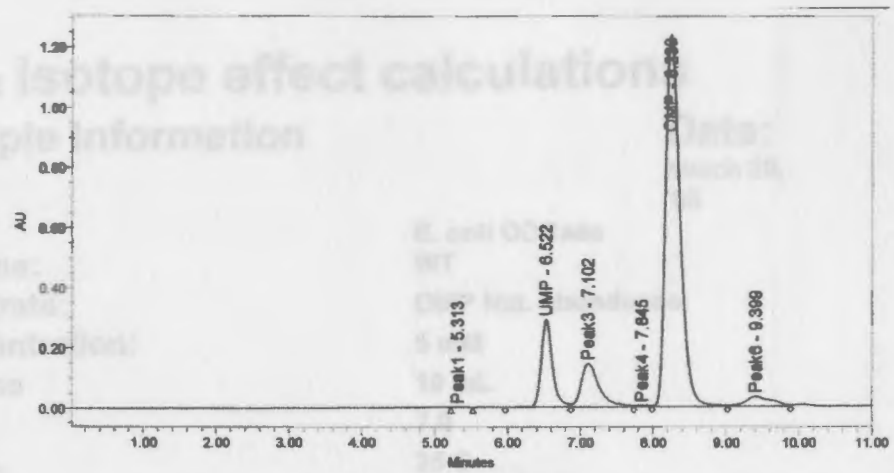

	Peak Name	RT (min)	Area (μV*sec)	% Area	Height (μV)	% Height
1	Peak1	5.313	10411	0.04	1506	0.09
2	UMP	6.522	3109806	13.28	292441	17.10
3	Peak3	7.102	2460987	10.51	144587	8.45
4	Peak4	7.845	59365	0.25	4698	0.27
5	OMP	8.233	16942920	72.34	1234639	72.20
6	Peak6	9.399	837536	3.58	32206	1.88

Figure H-3a. HPLC data (absorbance at 270 nm) to determine fraction of reaction for ODCase isotope effect measurement, natural abundance OMP, pH 7.0, trial #2.

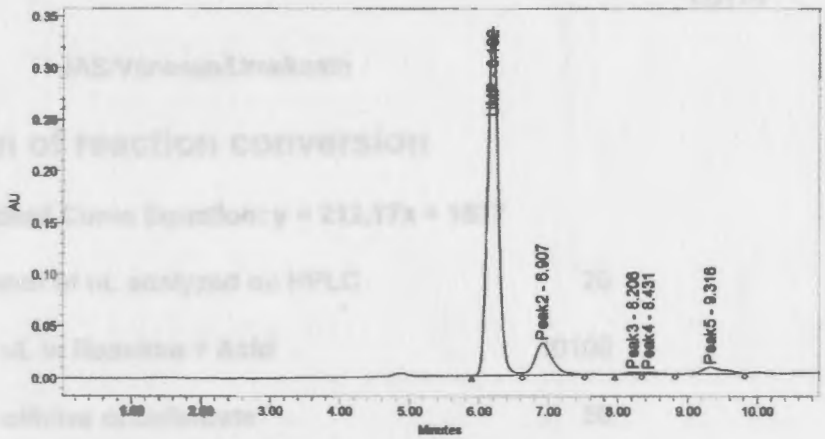

	Peak Name	RT (min)	Area (μV*sec)	% Area	Height (μV)	% Height
1	UMP	6.162	3630450	83.41	338814	89.44
2	Peak2	6.907	526926	12.11	30312	8.05
3	Peak3	8.206	23936	0.55	1888	0.50
4	Peak4	8.431	22956	0.53	1507	0.40
5	Peak5	9.316	148355	3.41	6089	1.61

Figure H-3b. HPLC data (absorbance at 270 nm) to verify complete reaction for ODCase isotope effect measurement, natural abundance OMP, pH 7.0, trial #2.

CO_2 Isotope effect calculations

Sample Information

Date: March 29, '06

Enzyme:	**E. coli ODCase WT**
Substrate:	**OMP Nat. abundance**
Concentration:	**5 mM**
Volume	**10 mL**
pH	**7.0**
Temp.	**25 C**
Buffer	**50 mM MOPS**
Reaction time	**5 min.**
Enzyme	**83 mg**

Fraction reaction (0.0 - 1.0)	0.075	
		1000 + δ
Delta value (partial rxn)	24.6	1024.6
Delta value (100% conversion)	41.3	1041.3
Isotope effect	1.0170	

User JAS/Vanessa/Umakanth

Fraction of reaction conversion

UMP Standard Curve Equation: y = 212.17x + 1537

Enter Number of uL analyzed on HPLC	20
Enter # of uL in Reaction + Acid	10100
Enter # of uMoles of Substrate	50
Enter peak area/1000	33100
nmol in HPLC sample	7.41
Fraction of Reaction	0.075

Table H-3. Isotope ratio data for ODCase isotope effect measurement, natural abundance OMP, pH 7.0, trial #2.

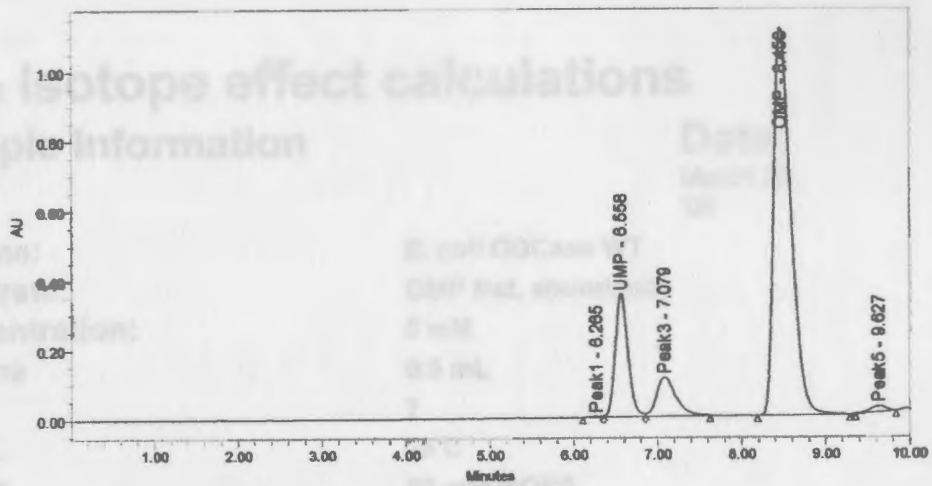

	Peak Name	RT (min)	Area (µV*sec)	% Area	Height (µV)	% Height
1	Peak1	6.265	24828	0.11	2754	0.17
2	UMP	6.558	3700608	17.12	354812	22.14
3	Peak3	7.079	1762924	8.16	110961	6.92
4	OMP	8.458	15897903	73.56	1117186	69.70
5	Peak5	9.627	225862	1.05	17207	1.07

Figure H-4a. HPLC data (absorbance at 264 nm) to determine fraction of reaction for ODCase isotope effect measurement, natural abundance OMP, pH 7.0, trial #3.

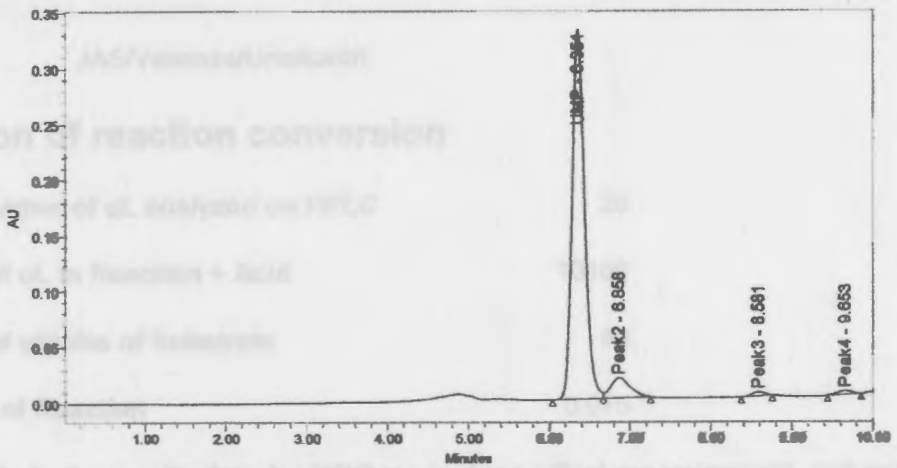

	Peak Name	RT (min)	Area (µV*sec)	% Area	Height (µV)	% Height
1	UMP	6.351	3499584	90.25	330207	93.13
2	Peak2	6.858	298079	7.69	17606	4.97
3	Peak3	8.581	38569	0.99	3546	1.00
4	Peak4	9.653	41530	1.07	3222	0.91

Figure H-4b. HPLC data (absorbance at 264 nm) to verify complete reaction for ODCase isotope effect measurement, natural abundance OMP, pH 7.0, trial #3.

CO_2 Isotope effect calculations

Sample Information

Date: March 30, '06

Enzyme:	**E. coli ODCase WT**
Substrate:	**OMP Nat. abundance**
Concentration:	**5 mM**
Volume	**9.5 mL**
pH	**7**
Temp.	**25 C**
Buffer	**50 mM MOPS**
Reaction time	**6 min.**
Enzyme	**83 mg**

Fraction reaction (0.0 - 1.0)	0.189	
		1000 + δ
Delta value (partial rxn)	22.0	1022.0
Delta value (100% conversion)	46.7	1046.7
Isotope effect	1.0269	

User JAS/Vanessa/Umakanth

Fraction of reaction conversion

Enter Number of uL analyzed on HPLC	20
Enter # of uL in Reaction + Acid	10100
Enter # of uMoles of Substrate	50
Fraction of Reaction	0.075

Table H-4. Isotope ratio data for ODCase isotope effect measurement, natural abundance OMP, pH 7.0, trial #3.

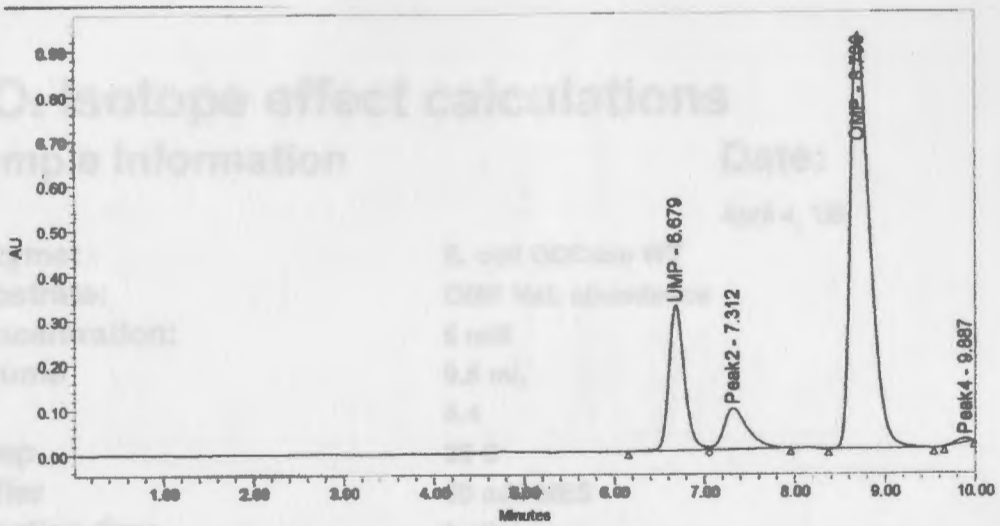

	Peak Name	RT (min)	Area (μV*sec)	% Area	Height (μV)	% Height
1	UMP	6.679	3819382	19.62	322938	23.99
2	Peak2	7.312	1659104	8.52	91387	6.79
3	OMP	8.700	13888893	71.35	923036	68.57
4	Peak4	9.887	99161	0.51	8823	0.66

Figure H-5a. HPLC data (absorbance at 264 nm) to determine fraction of reaction for ODCase isotope effect measurement, natural abundance OMP, pH 5.4, trial #4.

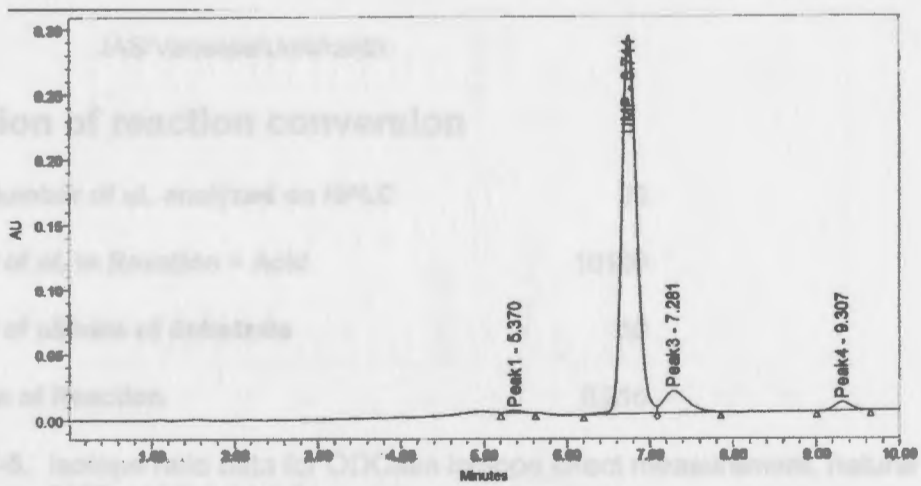

	Peak Name	RT (min)	Area (μV*sec)	% Area	Height (μV)	% Height
1	Peak1	5.370	17706	0.44	1612	0.51
2	UMP	6.744	3582955	89.17	290590	92.17
3	Peak3	7.281	326882	8.14	16588	5.26
4	Peak4	9.307	90661	2.26	6479	2.06

Figure H-5b. HPLC data (absorbance at 264 nm) to verify complete reaction for ODCase isotope effect measurement, natural abundance OMP, pH 7.0, trial #4.

CO_2 Isotope effect calculations

Sample Information

Date: April 4, '06

Enzyme:	**E. coli ODCase WT**
Substrate:	**OMP Nat. abundance**
Concentration:	**5 mM**
Volume	**9.5 mL**
pH	**5.4**
Temp.	**25 C**
Buffer	**50 mM MES**
Reaction time	**6 min.**
Enzyme	**166 mg**

		$\frac{1000 + \delta}{}$
Fraction reaction (0.0 - 1.0)	0.216	
Delta value (partial rxn)	70.2	1070.2
Delta value (100% conversion)	60.4	1060.4
Isotope effect	0.9896	

User JAS/Vanessa/Umakanth

Fraction of reaction conversion

Enter Number of uL analyzed on HPLC	20
Enter # of uL in Reaction + Acid	10100
Enter # of uMoles of Substrate	50
Fraction of Reaction	0.216

Table H-5. Isotope ratio data for ODCase isotope effect measurement, natural abundance OMP, pH 5.4, trial #4.

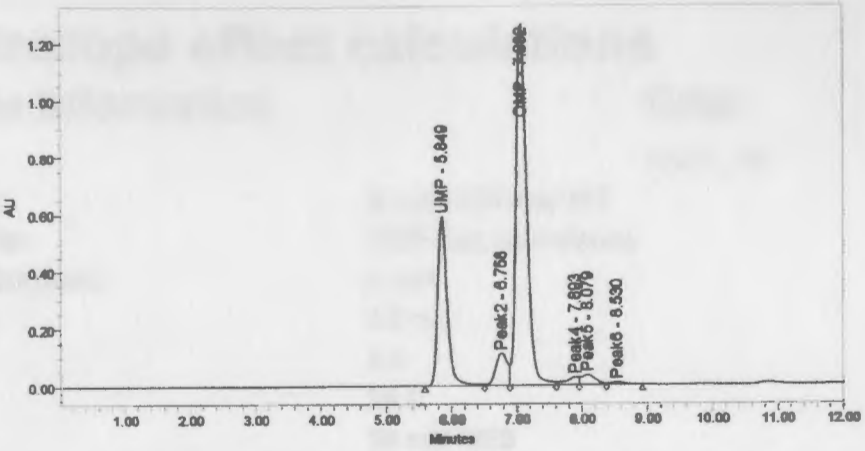

	Peak Name	RT (min)	Area (μV*sec)	% Area	Height (μV)	% Height
1	UMP	5.849	5885864	26.36	587935	28.99
2	Peak2	6.758	1352553	6.06	110214	5.43
3	OMP	7.062	14147361	63.37	1264141	62.33
4	Peak4	7.893	342869	1.54	26344	1.30
5	Peak5	8.079	498423	2.23	33160	1.63
6	Peak6	8.530	99368	0.45	6342	0.31

Figure H-6a. HPLC data (absorbance at 264 nm) to determine fraction of reaction for ODCase isotope effect measurement, natural abundance OMP, pH 5.4, trial #5.

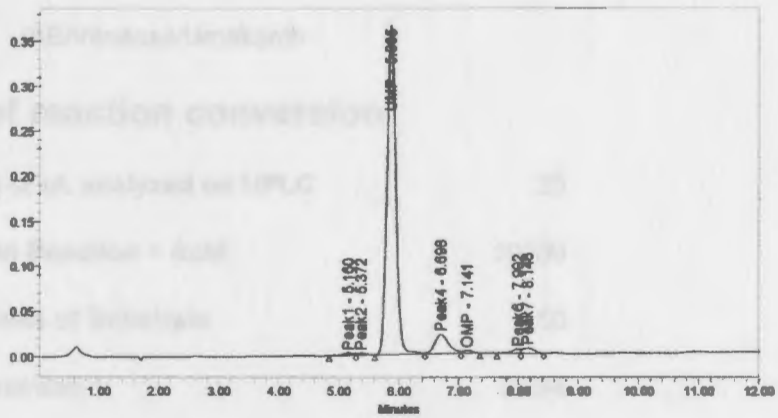

	Peak Name	RT (min)	Area (μV*sec)	% Area	Height (μV)	% Height
1	Peak1	5.160	30013	0.71	2305	0.57
2	Peak2	5.372	20470	0.48	1870	0.46
3	UMP	5.865	3707114	87.28	365089	90.42
4	Peak4	6.698	338344	7.97	21032	5.21
5	OMP	7.141	30948	0.73	3022	0.75
6	Peak6	7.992	43880	1.03	4588	1.13
7	Peak7	8.146	76887	1.81	5870	1.45

Figure H-6b. HPLC data (absorbance at 264 nm) to verify complete reaction for ODCase isotope effect measurement, natural abundance OMP, pH 7.0, trial #5.

CO_2 Isotope effect calculations

Sample Information

Date: April 5, '06

Enzyme:	**E. coli ODCase WT**
Substrate:	**OMP Nat. abundance**
Concentration:	**5 mM**
Volume	**9.5 mL**
pH	**5.4**
Temp.	**25 C**
Buffer	**50 mM MES**
Reaction time	**5 min.**
Enzyme	**166 mg**

		$\frac{1000 + \delta}{}$
Fraction reaction (0.0 - 1.0)	0.294	
Delta value (partial rxn)	48.3	1048.3
Delta value (100% conversion)	72.6	1072.6
Isotope effect	1.0277	

User JAS/Vanessa/Umakanth

Fraction of reaction conversion

Enter Number of uL analyzed on HPLC	20
Enter # of uL in Reaction + Acid	10100
Enter # of uMoles of Substrate	50
Fraction of Reaction	0.294

Table H-6. Isotope ratio data for ODCase isotope effect measurement, natural abundance OMP, pH 5.4, trial #5.

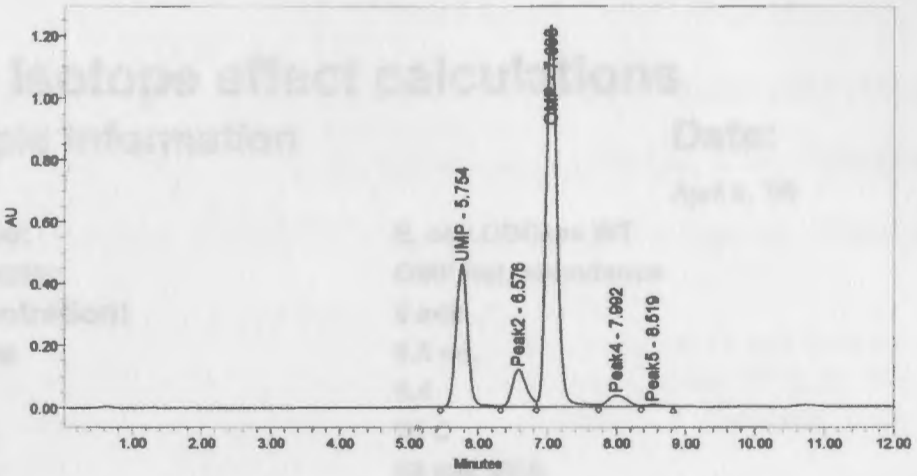

	Peak Name	RT (min)	Area (μV*sec)	% Area	Height (μV)	% Height
1	UMP	5.754	5347757	25.06	462179	25.00
2	Peak2	6.576	1704779	7.99	118228	6.39
3	OMP	7.033	13493517	63.24	1227789	66.41
4	Peak4	7.992	704826	3.30	34731	1.88
5	Peak5	8.519	85301	0.40	5858	0.32

Figure H-7a. HPLC data (absorbance at 264 nm) to determine fraction of reaction for ODCase isotope effect measurement, natural abundance OMP, pH 5.4, trial #6.

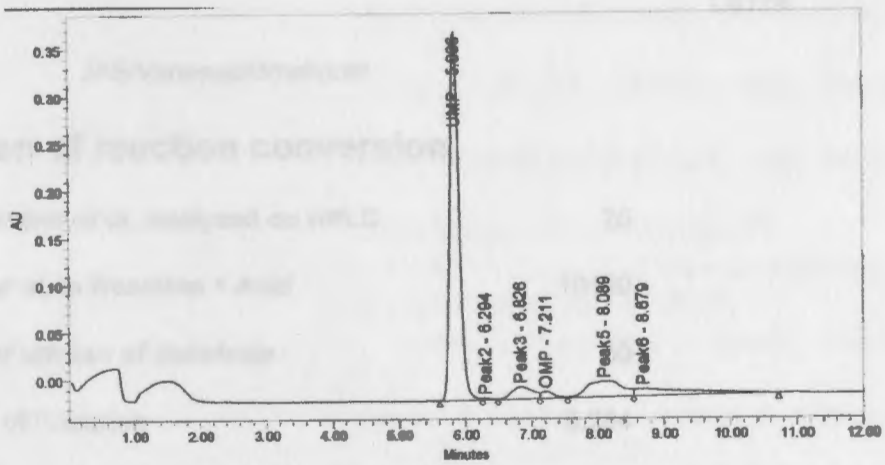

	Peak Name	RT (min)	Area (μV*sec)	% Area	Height (μV)	% Height
1	UMP	5.836	3718289	71.69	388640	89.58
2	Peak2	6.294	14546	0.28	1545	0.36
3	Peak3	6.826	281404	5.43	12715	2.93
4	OMP	7.211	90890	1.75	7202	1.66
5	Peak5	8.089	607415	11.71	16158	3.72
6	Peak6	8.679	474401	9.15	7603	1.75

Figure H-7b. HPLC data (absorbance at 264 nm) to verify complete reaction for ODCase isotope effect measurement, natural abundance OMP, pH 7.0, trial #6.

CO_2 Isotope effect calculations

Sample Information

Date: April 5, '06

Enzyme:	**E. coli ODCase WT**
Substrate:	**OMP Nat. abundance**
Concentration:	**5 mM**
Volume	**9.5 mL**
pH	**5.4**
Temp.	**25 C**
Buffer	**50 mM MES**
Reaction time	**4 min.**
Enzyme	**166 mg**

Fraction reaction (0.0 - 1.0)	0.284	
		$\frac{1000 + \delta}{}$
Delta value (partial rxn)	58.3	1058.3
Delta value (100% conversion)	69.7	1069.7
Isotope effect	1.0128	

User JAS/Vanessa/Umakanth

Fraction of reaction conversion

Enter Number of uL analyzed on HPLC	20
Enter # of uL in Reaction + Acid	10100
Enter # of uMoles of Substrate	50
Fraction of Reaction	0.284

Table H-7. Isotope ratio data for ODCase isotope effect measurement, natural abundance OMP, pH 5.4, trial #6.

References

[1] M.H. O'Leary. in (Sigman, D.S., ed.) The Enzymes: Mechanisms in Catalysis, Academic Press, San Diego 1992, pp. 235-69.

[2] T. Li, A.L. Walker, H. Iwaki, Y. Hasegawa and A. Liu, J Am Chem Soc 127 (2005) 12282-90.

[3] Y. Egashira, H. Kouhashi, T. Ohta and H. Sanada, J. Nutr. Sci. Vitaminol. 42 (1996) 173-83.

[4] A.H. Mehler, J. Biol. Chem. 218 (1956) 241-254.

[5] Y. Nishizuka, A. Ichiyama and O. Hayaishi. in (Tabor, H. and Tabor, C.W., eds.) Methods Enzymol., Academic Press, New York ; London 1970, pp. 466.

[6] S. Fukuoka, K. Ishiguro, K. Yanagihara, A. Tanabe, Y. Egashira, H. Sanada and K. Shibata, J Biol Chem 277 (2002) 35162-7.

[7] A. Tanabe, Y. Egashira, S. Fukuoka, K. Shibata and H. Sanada, Biochem J 361 (2002) 567-75.

[8] A. Radzicka and R. Wolfenden, Science 267 (1995) 90-3.

[9] J.K. Lee and D.J. Tantillo, Orotidine monophosphate decarboxylase : a mechanistic dialogue, Springer, Berlin, 2004.

[10] N. Wu, D. Christendat, A. Dharamsi and E.F. Pai, Acta Crystallogr D Biol Crystallogr 56 (Pt 7) (2000) 912-4.

[11] B.G. Miller, A.M. Hassell, R. Wolfenden, M.V. Milburn and S.A. Short, Proc Natl Acad Sci U S A 97 (2000) 2011-6.

[12] P. Harris, J.C. Navarro Poulsen, K.F. Jensen and S. Larsen, Biochemistry 39 (2000) 4217-24.

[13] T.C. Appleby, C. Kinsland, T.P. Begley and S.E. Ealick, Proc Natl Acad Sci U S A 97 (2000) 2005-10.

[14] J.A. Smiley, P. Paneth, M.H. O'Leary, J.B. Bell and M.E. Jones, Biochemistry 30 (1991) 6216-23.

[15] T. Muraki, M. Taki, Y. Hasegawa, H. Iwaki and P.C. Lau, Appl Environ Microbiol 69 (2003) 1564-72.

[16] W. Koontz and R. Shiman, J. Biol. Chem. 251 (1976) 368-77.

[17] P. Malherbe, C. Kohler, M. Da Prada, G. Lang, V. Kiefer, R. Schwarcz, H.W. Lahm and A.M. Cesura, J Biol Chem 269 (1994) 13792-7.

[18] V. Calderone, M. Trabucco, V. Menin, A. Negro and G. Zanotti, Biochim Biophys Acta 1596 (2002) 283-92.

[19] O. Kurnasov, V. Goral, K. Colabroy, S. Gerdes, S. Anantha, A. Osterman and T.P. Begley, Chemistry & Biology 10 (2003) 1195-1204.

[20] J.I. Ehrlich, C.-C. Hwang, P.F. Cook and J.S. Blanchard, J. Am. Chem. Soc. 121 (1999) 6966-6967.

[21] M.H. O'Leary. Methods in Enzymology, Academic Press, New York 1980, pp. 83-104.

[22] J.P. Jones, P.M. Weiss and W.W. Cleland, Biochemistry 30 (1991) 3634-9.

[23] H.K. Jensen, N. Mikkelsen and J. Neuhard, Protein Expression and Purification 10 (1997) 356 - 364.

[24] B.J. DelFraino. pp. 44 leaves, Youngstown State University. 2003.

[25] T. Ueda, M. Yamamoto, A. Yamane, M. Imazawa and H. Inoue, J. Carbohydr., Nucleosides, Nucleotides 5 (1978) 261-71.

[26] A.A. Axhemi. in Department of Chemistry, pp. 53, Youngstown State University 2005.